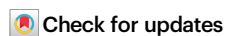



# Galactooligosaccharides and *Limosilactobacillus reuteri* synergistically alleviate gut inflammation and barrier dysfunction by enriching *Bacteroides acidifaciens* for pentadecanoic acid biosynthesis

Received: 16 February 2024

Accepted: 1 October 2024

Published online: 28 October 2024



Yujun Wu<sup>1</sup>, Xiangyu Zhang<sup>1</sup>, Xiaoyi Liu<sup>1</sup>, Zhenguo Zhao<sup>2</sup>, Shiyu Tao<sup>3</sup>, Qian Xu<sup>1</sup>, Jinbiao Zhao<sup>1</sup>, Zhaolai Dai<sup>1</sup>, Guolong Zhang<sup>1</sup> <sup>4</sup>, Dandan Han<sup>1</sup> <sup>1</sup> & Junjun Wang<sup>1</sup> ✉

Ulcerative colitis (UC) is a debilitating inflammatory bowel disease characterized by intestinal inflammation, barrier dysfunction, and dysbiosis, with limited treatment options available. This study systematically investigates the therapeutic potential of a synbiotic composed of galactooligosaccharides (GOS) and *Limosilactobacillus reuteri* in a murine model of colitis, revealing that GOS and *L. reuteri* synergistically protect against intestinal inflammation and barrier dysfunction by promoting the synthesis of pentadecanoic acid, an odd-chain fatty acid, from *Bacteroides acidifaciens*. Notably, the synbiotic, *B. acidifaciens*, and pentadecanoic acid are each capable of suppressing intestinal inflammation and enhancing tight junction by inhibiting NF- $\kappa$ B activation. Furthermore, similar reduction in *B. acidifaciens* and pentadecanoic acid levels are also observed in the feces from both human UC patients and lipopolysaccharide-induced intestinal inflammation in pigs. Our findings elucidate the protective mechanism of the synbiotic and highlight its therapeutic potential, along with *B. acidifaciens* and pentadecanoic acid, for UC and other intestinal inflammatory disorders.

Ulcerative colitis (UC) is an inflammatory bowel disease (IBD), but its etiology and pathogenesis remain enigmatic<sup>1</sup>. Emerging evidence emphasizes its strong association with intestinal inflammation, barrier dysfunction, and dysbiosis<sup>2</sup>. However, few preventive and therapeutic options are currently available for UC. Dietary intervention stands as a primary strategy for alleviating UC symptoms, with prebiotics, probiotics, and synbiotics showing promise due to their reported ability to modify intestinal microbiota, modulate immune response, and

enhance barrier function<sup>3–5</sup>. A comprehensive understanding of the underlying protective mechanisms of these interventions may provide better options for treating UC.

Galactooligosaccharides (GOS) and *Limosilactobacillus reuteri* are well-known prebiotic and probiotic, respectively, with demonstrated benefits in microbial balance and intestinal barrier function<sup>6,7</sup>. We previously showed that dietary GOS enhances intestinal barrier function in *Salmonella*-challenged mice by selectively enriching three

<sup>1</sup>State Key Laboratory of Animal Nutrition and Feeding, College of Animal Science and Technology, China Agricultural University, Beijing 100193, China.

<sup>2</sup>Department of General Surgery, Jiangyin People's Hospital Affiliated to Nantong University, Jiangsu 214400, China. <sup>3</sup>College of Animal Sciences and Technology, Huazhong Agricultural University, Wuhan 430070, China. <sup>4</sup>Department of Animal and Food Sciences, Oklahoma State University, Stillwater 74078, USA. ✉e-mail: [wangjj@cau.edu.cn](mailto:wangjj@cau.edu.cn)

lactobacilli, including *L. reuteri*<sup>8</sup>. Notably, *L. reuteri* can utilize GOS as a carbon resource, providing the foundation for synbiotic development<sup>9</sup>. However, the synergistic mechanisms between GOS and *L. reuteri* in alleviating inflammation and enhancing barrier function remain unexplored. It is important to identify the intestinal bacteria and metabolites regulated by the synbiotic.

This study presents compelling evidence that the combination of GOS and *L. reuteri* mitigates intestinal inflammation and barrier dysfunction by enriching *Bacteroides acidifaciens* and promoting the synthesis of pentadecanoic acid (C15:0), an odd-chain fatty acid. In a mouse model of dextran sulfate sodium (DSS)-induced colitis, we observed a significant reduction in C15:0 level, which could be restored by the synbiotic-enriched *B. acidifaciens*. Importantly, similar impairments in *B. acidifaciens* and C15:0 synthesis were also observed in other intestinal inflammation conditions, such as UC and a porcine model of LPS-induced inflammation. Administration of *B. acidifaciens* or C15:0 conferred significant protection against DSS-induced colitis by suppressing inflammatory cytokine production while enhancing tight junction protein expression. Collectively, our findings uncover a major mechanism of action of GOS and *L. reuteri* and also offer a promising avenue for mitigating intestinal inflammation and barrier dysfunction in UC and potentially other intestinal inflammatory diseases.

## Results

### Synbiotic GOS and *L. reuteri* are highly effective in ameliorating intestinal inflammation and barrier dysfunction while enriching *Bacteroides acidifaciens*

*L. reuteri* can utilize GOS if provided as the only carbon resource, implying a synergistic action between *L. reuteri* and GOS<sup>9</sup>. To study the impact of a synbiotic consisting of GOS and *L. reuteri* on intestinal inflammation and barrier function, we administered GOS and *L. reuteri* separately or in combination to mice for four weeks, followed by DSS treatment for another week (Fig. 1a). The results indicated that the synbiotic, but not GOS or *L. reuteri* alone, markedly reversed body weight loss (Fig. 1b) and shortening of the colon (Fig. 1c), while preserving the integrity of the colon mucosa (Fig. 1d). Furthermore, the synbiotic significantly alleviated intestinal damage (Fig. 1e), reversed DSS-induced suppression of tight junction proteins Claudin-1, Occludin, and ZO-1 (Fig. 1f), and attenuated intestinal inflammation by decreasing pro-inflammatory cytokines TNF- $\alpha$ , IL-1 $\beta$ , and IL-6 (Fig. 1g).

While DSS caused an obvious shift in the colonic microbiota composition, the synbiotic led to further alterations without restoring it back to normal (Fig. 1h). A closer examination revealed DSS caused a drastic reduction of *Bacteroides* in the colon of healthy mice, while the synbiotic restored *Bacteroides* in DSS-treated mice (Fig. 1i, j). Additionally, *Bacteroides acidifaciens* and *B. xylanisolvens* were specifically enriched among *Bacteroides* species (Fig. S1a). In contrast, GOS or *L. reuteri* alone failed to enrich *B. acidifaciens* in DSS-treated mice (Fig. 1k). Shotgun metagenomic sequencing further validated the increase in relative abundance of *B. acidifaciens* following synbiotic intervention (Fig. S1b–f). Moreover, random forest analysis revealed *B. acidifaciens* to be ranked the most important species that distinguished the intestinal microbiotas with and without synbiotic intervention (Fig. 1l).

To further evaluate whether other strains of *L. reuteri* exhibit similar anti-inflammatory and *B. acidifaciens*-enriching effects, we administered two other strains of *L. reuteri* isolated from the mouse feces by our lab in DSS-treated mice (Fig. S2a). One strain, *L. reuteri* #1, demonstrated beneficial effects comparable to *L. reuteri* BNCC 186135, used above in the synbiotic, on DSS-induced body weight loss (Fig. S2b), intestinal inflammation (Fig. S2c–e), barrier function (Fig. S2f), and serum cytokine levels (Fig. S2g). In contrast, the other strain had minimal impact. Additionally, *B. acidifaciens* was significantly enriched in DSS-treated mice supplemented with *L. reuteri*

#1, but not with strain #2 (Fig. S2h), suggesting a strain-specific effect. Therefore, it is possible to identify more potent strains to be used in the synbiotic for treating UC if screening additional *L. reuteri* strains.

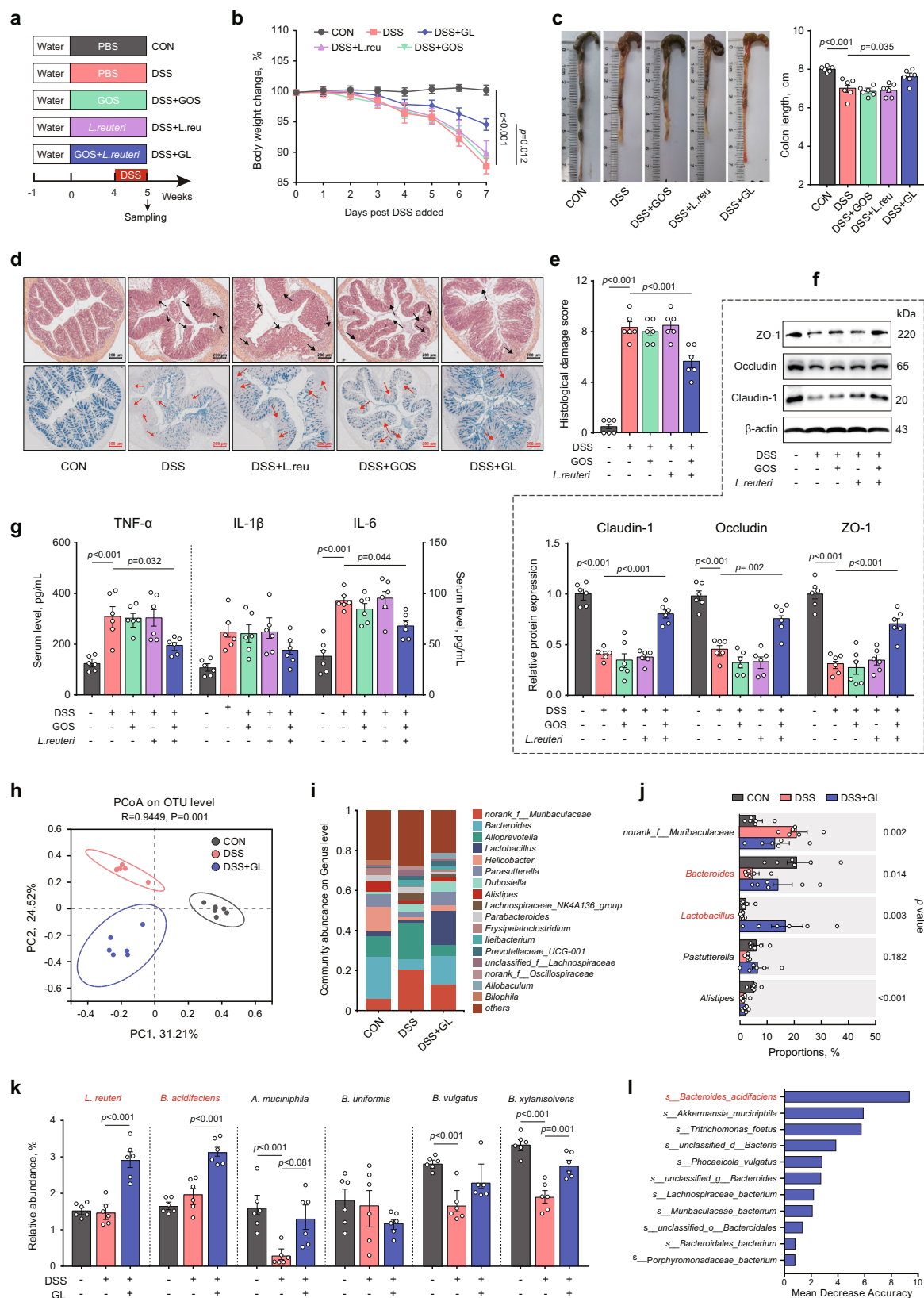
To further identify the key metabolites produced specifically by the synbiotic to be responsible for *B. acidifaciens* enrichment, we examined differentially abundant metabolites in the feces of DSS-treated mice administered with GOS, *L. reuteri*, or the synbiotic. Our results revealed that  $\beta$ -alanine, N-acetyl-D-glucosamine, 4-methylhexanoic acid, C15:0, and myristic acid were the top five metabolites significantly enriched in response to the synbiotic but not to GOS or *L. reuteri* alone (Fig. S3a, b). To determine which metabolites preferentially support the growth of *B. acidifaciens*, we cultured mouse cecal microbiota anaerobically with GOS, *L. reuteri*, the synbiotic, or each of the differentially enriched metabolites. The results showed that only N-acetyl-D-glucosamine significantly increased the relative abundance of *B. acidifaciens* in the culture medium, approaching the efficacy of the synbiotic (Fig. S3c). Additionally, N-acetyl-D-glucosamine specifically enhanced the growth of *B. acidifaciens* when glucose was replaced (Fig. S3d). Taken together, N-acetyl-D-glucosamine is the major metabolite derived from the synbiotic GOS and *L. reuteri* responsible for the enrichment of *B. acidifaciens*.

### *B. acidifaciens* is enriched in recipient mice by FMT with synbiotic-derived microbiota

To assess whether the fecal microbiota from the synbiotic-supplemented mice is capable of alleviating intestinal inflammation and barrier dysfunction, FMT was performed with intestinal microbiota-depleted recipient mice (Fig. 2a). Synbiotic-derived microbiota, rather than the control microbiota, effectively attenuated the body weight loss (Fig. 2b), the colon length (Fig. 2c), and the damage to the intestinal mucosal surface (Fig. 2d, e) of DSS-treated mice. Furthermore, the serum levels of pro-inflammatory cytokines, including TNF- $\alpha$ , IL-1 $\beta$ , and IL-6, were significantly suppressed in DSS-treated mice in response to the synbiotic (Fig. 2f), and the expressions of tight junction proteins, such as Claudin-1 and Occludin, were substantially restored (Fig. 2g). Additionally, FMT altered the fecal microbiota structure of recipient mice (Fig. 2h). At the genus level, *Bacteroides* and *Lactobacillus* were both increased in mice receiving the synbiotic-derived microbiota (Fig. 2i, j). At the species level, *B. acidifaciens*, rather than *B. xylanisolvens*, was successfully colonized the intestine following FMT (Fig. 2k), suggesting that *B. acidifaciens* may be potentially important in protecting against intestinal inflammation and barrier dysfunction in DSS-treated mice.

### *B. acidifaciens* protects against intestinal inflammation and barrier dysfunction

To directly assess the role of *B. acidifaciens* in protecting against intestinal inflammation and barrier dysfunction, *B. acidifaciens* was inoculated into mice for two weeks, followed by one week of DSS treatment to induce colitis (Fig. 3a). *B. acidifaciens* significantly attenuated DSS-induced intestinal damage as shown in body weight loss, the colon length, intestinal morphology, and histological damage score (Fig. 3b–e). Oral administration of *B. acidifaciens* also partially restored the protein expressions of tight junctions (Fig. 3f) and suppressed protein expressions of pro-inflammatory cytokines (Fig. 3g). These results confirmed that *B. acidifaciens* enriched by GOS and *L. reuteri* protects against intestinal inflammation and barrier dysfunction. A valuation of a second strain of *B. acidifaciens* in DSS-treated mice revealed similar protective effects on reversing body weight loss, intestinal inflammation, barrier dysfunction, and serum cytokine increase (Fig. S4a–h). Additional *B. acidifaciens* strains may be tested to determine a strain-specific effect and the possibility of identifying more effective probiotic candidates.



### Synbiotic GOS and *L. reuteri* enhance the synthesis of pentadecanoic acid (C15:0) to alleviate intestinal inflammation and barrier dysfunction

To explore the protective role of the synbiotic-derived metabolites in the restoration of intestinal barrier dysfunction, bacterial cell-free supernatant was prepared from the feces of mice fed standard chow or

supplemented with the synbiotic, followed by oral administration to DSS-treated mice (Fig. 4a). The results showed that the supernatant derived from synbiotic-supplemented mice, but not standard chow-fed mice, significantly reversed the body weight loss of DSS-treated mice (Fig. 4b). The colon length (Fig. 4c), mucosal integrity (Fig. 4d), histological damage score (Fig. 4e), goblet cell number (Fig. 4f), tight

**Fig. 1 | Synbiotic galactooligosaccharides (GOS) and *L. reuteri* effectively ameliorates intestinal inflammation and barrier dysfunction and enriches *Bacteroides acidifaciens*.** After a week of acclimation, 8-week-old male C57BL/6 J mice ( $n = 6$  per group) were supplemented with GOS (5%, w/w) to the diet for five weeks with or without daily oral gavage of  $2 \times 10^8$  CFU *L. reuteri*. Colitis was induced by providing 3% DSS in drinking water in the final week. **a, b** Study design and body weight change in DSS-treated mice supplemented with GOS and *L. reuteri* individually or in combination. **c–e** The length, H&E staining, Alcian blue staining, and histological damage score of the colon in DSS-treated mice supplemented with GOS and *L. reuteri* individually or in combination. **f, g** Relative protein expressions of tight junction proteins in the colon and serum concentrations of pro-inflammatory cytokines in DSS-treated mice supplemented with GOS and *L. reuteri*

individually or in combination. **h–j** Principal coordinates analysis (PCoA) of weighted UniFrac distances, microbiota composition, and differential abundance of the fecal microbiota at the genus. **k** Relative abundance of *B. acidifaciens* and *A. muciniphila* in DSS-treated mice supplemented with GOS and *L. reuteri* individually or in combination detected by RT-qPCR with specific primers. **l** Random forest analysis of the shotgun metagenomic sequencing data for the most important discriminating bacterial taxon between treatments. Samples for western blot were derived from the same experiment and gels/blots were processed in parallel. The Kruskal–Wallis test and post-hoc Dunn's was used for microbial analysis, and one-way ANOVA with Tukey's test was used for statistical analysis of all other parameters. Data were presented as mean  $\pm$  SEM. Source data were provided as a Source Data file.

junction protein expressions (Fig. 4g), and serum pro-inflammatory cytokine levels (Fig. 4h) were also restored by the synbiotic-derived intestinal supernatant, suggesting that the intestinal metabolites produced in response to synbiotic administration contribute to alleviating intestinal inflammation and barrier dysfunction.

To identify the possible metabolites responsible for disease alleviation, targeted metabolomics was conducted with the fecal bacterial cell-free supernatants of DSS-treated mice supplemented with or without GOS, *L. reuteri*, or their combination. A total of 35 metabolites from 306 representative metabolites of different classes were found to be differentially enriched in response to GOS and/or *L. reuteri* (Fig. 5a). Among them, pentadecanoic acid (C15:0) was the most significantly down-regulated following DSS treatment and up-regulated in response to the synbiotic administration as evidenced by the lowest adjusted p-value (Fig. 5b, c). Indeed, C15:0 was increased in the feces of DSS-treated mice following synbiotic administration (Fig. 5d). Interestingly, 9-pentadecanoic acid, a less abundant C15:0 isoform, was also similarly increased in response to the synbiotic (Fig. 5e). Consistently, fecal concentrations of C15:0 were also increased in DSS-treated mice transplanted with fecal microbiota (Fig. 5f), fecal bacterial cell-free supernatant (Fig. 5g), or *B. acidifaciens* (Fig. 5h). These results collectively suggested that C15:0 may be a key metabolite produced by the synbiotic and responsible for alleviating intestinal inflammation and barrier dysfunction.

### ***B. acidifaciens* synthesizes pentadecanoic acid (C15:0) to protect against the intestinal inflammation and barrier dysfunction**

To identify whether C15:0 can be directly synthesized by *B. acidifaciens*, we cultured *B. acidifaciens* in the presence of GOS and *L. reuteri* individually or in combination. Elevated C15:0 was observed in the culture supernatant of *B. acidifaciens*, and importantly, the combination of GOS and *L. reuteri* markedly increased the amount of C15:0 when co-cultured with *B. acidifaciens*, while either alone only had a marginal effect (Fig. 6a). To directly confirm whether *B. acidifaciens* has the capacity to synthesize C15:0, we performed whole-genome sequencing of *B. acidifaciens* and found it to encode 39 genes involved in lipid metabolism (Fig. S5). Notably, all key genes for biosynthesis of C15:0 were present (Fig. 6b), suggesting that *B. acidifaciens* is a C15:0-producing bacterium.

To further examine how those major C15:0-synthesizing genes are regulated in the synbiotic-supplemented mice, we performed shotgun metagenomics sequencing and revealed that four genes, namely *fabK*, *acrC*, *fabF* and *FATA*, were downregulated by DSS, but restored upon the synbiotic supplementation (Fig. 6c), suggesting that the combination of GOS and *L. reuteri* may accelerate C15:0 biosynthesis through enriching *B. acidifaciens*. Indeed, among all differentially enriched fatty acids, only C15:0 showed a significantly positive correlation with *B. acidifaciens* in DSS-treated mice supplemented with the synbiotic (Fig. 6d). Additionally, the fecal concentrations of C15:0 were positively correlated with *B. acidifaciens* in recipient mice administered with the fecal microbiota of the synbiotic-supplemented mice (Fig. 6e) or direct *B. acidifaciens* (Fig. 6f). These results collectively suggested

that C15:0 is a metabolite synthesized by *B. acidifaciens* that may be involved in the protection of mice from DSS-induced intestinal damage.

### **Pentadecanoic acid (C15:0) ameliorates intestinal inflammation and barrier dysfunction by activating FATP4 and suppressing NF- $\kappa$ B activation**

To directly verify the protection of *B. acidifaciens*-derived C15:0 against the intestinal barrier dysfunction, C15:0 was orally administered daily to mice for three weeks, followed by DSS treatment for another week (Fig. 7a). The results showed that C15:0 significantly attenuated the body weight loss (Fig. 7b) and damage to the colon (Fig. 7c–f), upregulated tight junction protein expressions (Fig. 7g) and suppressed mRNA expressions of pro-inflammatory cytokines (Fig. 7h). Furthermore, C15:0 restored tight junction protein expressions and significantly downregulated LPS-induced pro-inflammatory cytokine expressions in both murine MODE-K cells (Fig. 7i–k) and human Caco-2 cells (Fig. S6), suggesting that C15:0 is broadly anti-inflammatory and protects barrier function by suppressing inflammatory cytokine synthesis.

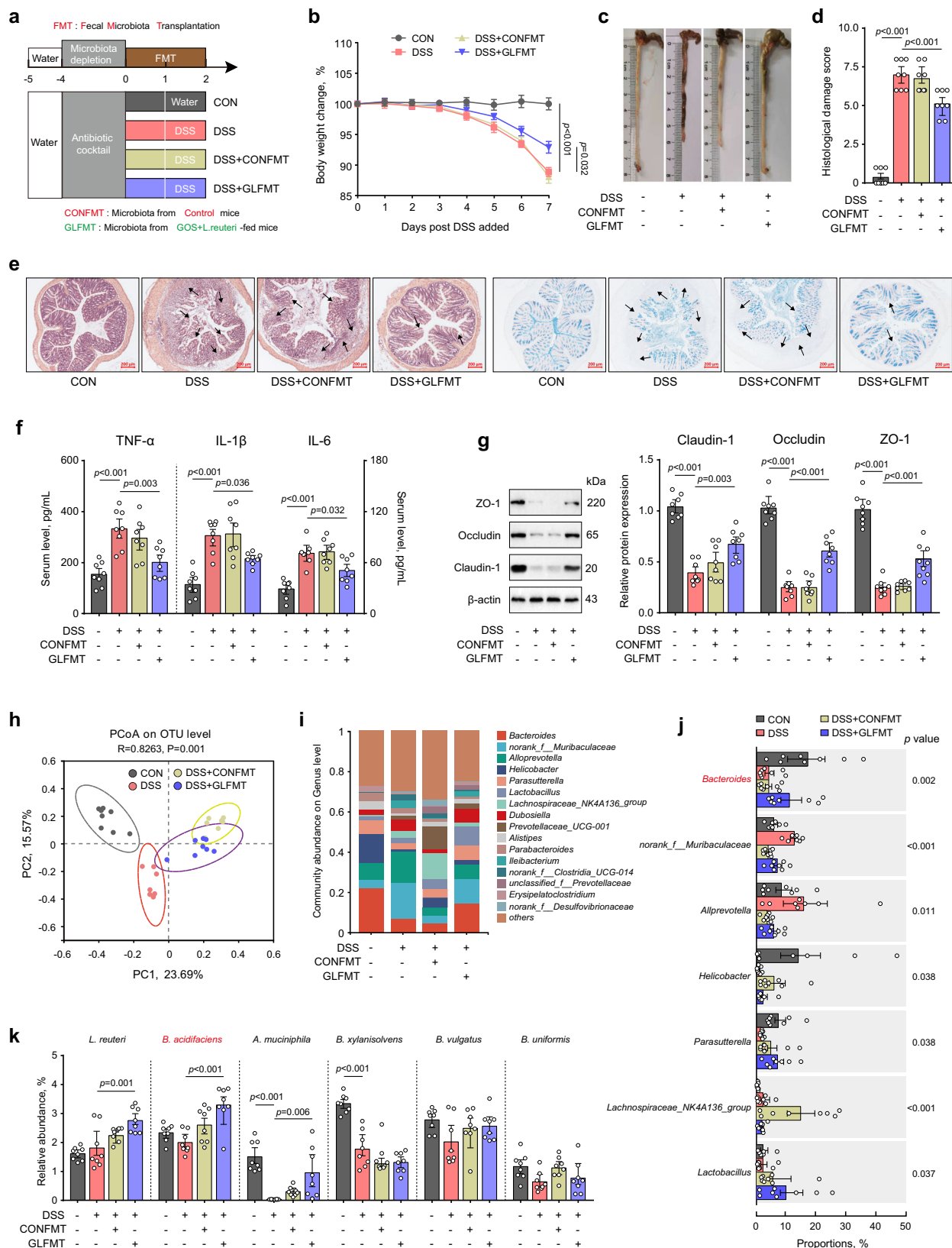
To further uncover the underlying mechanisms of C15:0-mediated protection of the intestinal barrier integrity, we performed RNA-seq of the colon tissue of DSS-treated mice with or without C15:0 administration (Fig. 8a). The results showed that C15:0 inhibited multiple inflammation-related pathways (Fig. 8b). RT-qPCR further confirmed C15:0-mediated suppression of the mRNA expression of pro-inflammatory cytokines *IL-1 $\alpha$* , *CCL2*, *NLRP3*, *CXCL1* and *IL-18* in the colon of DSS-treated mice (Fig. S7a–d). Mechanically, C15:0 suppressed NF- $\kappa$ B activation in DSS-treated mice (Fig. 8c) and LPS-challenged MODE-K cells (Fig. 8d), as evidenced by reduced phosphorylation of NF- $\kappa$ B p65. Consistently, phosphorylation of NF- $\kappa$ B p65 were also decreased in DSS-treated mice administered with the synbiotic (Fig. 8e), fecal microbiota (Fig. 8f), fecal bacterial cell-free supernatant (Fig. 8g), or *B. acidifaciens* (Fig. 8h).

Additionally, fatty acid transport protein 4 (FATP4/Slc27a4), a major long-chain fatty acid transporter and fatty acyl-CoA synthase<sup>10,11</sup>, was suppressed in the colon of DSS-treated mice (Fig. S8a), LPS-challenged human Caco-2 cells (Fig. S8b), and murine MODE-K cells (Fig. S8c), but were largely restored by C15:0 administration. Furthermore, C15:0-mediated restoration of tight junction protein expression and suppression of pro-inflammatory cytokines in LPS-treated MODE-K cells were markedly reversed by an FATP4 inhibitor (Fig. S8d–f). These results suggested that the anti-inflammatory and barrier protective properties of C15:0 were mediated through FATP4 and suppression of NF- $\kappa$ B activation.

### ***B. acidifaciens* and pentadecanoic acid are downregulated in UC patients and LPS-challenged piglets**

We observed a significant decrease in *B. acidifaciens* and C15:0 levels in DSS-treated mice, which was restored by GOS and *L. reuteri* administration. To confirm the clinical relevance of our findings in other intestinal inflammatory diseases, we initially examined the





relative abundance of *B. acidifaciens* in a cohort of 15 healthy donors and 11 UC patients admitted to Jiangyin People's Hospital affiliated with Nantong University (Jiangsu, China) in 2023. RT-qPCR revealed a significant reduction of *B. acidifaciens* in the feces of UC patients compared to healthy individuals (Fig. 9a). The concentration of C15:0 was also significantly reduced in UC patients (Fig. 9b).

Additionally, fecal concentrations of C15:0 positively correlated with the abundance of *B. acidifaciens* in the feces of both UC and healthy individuals (Fig. 9c). Similarly, LPS challenge induced obvious gut inflammation in piglets (Fig. S9), associated with significant reductions of both *B. acidifaciens* (Fig. 9d) and C15:0 levels (Fig. 9e) in the feces. A strong positive association was also

**Fig. 2 | *B. acidifaciens* is enriched in DSS-treated mice transplanted with the fecal microbiota of synbiotic-supplemented mice.** After a week of acclimation, the intestinal microbiota of 4-week-old male C57BL/6J mice ( $n = 8$  per group) were depleted with a cocktail of antibiotics for four weeks, followed by two-week daily gavage of PBS or the fecal microbiota prepared from the mice fed standard chow (CONFMT) or GOS/*L. reuteri* (GLFMT). Colitis was induced in mice by providing 3% DSS in the final week. **a, b** Study design and body weight change in DSS-treated mice with/without treatment with CONFMT or GLFMT. **c–e** The length, H&E staining, Alcian blue staining, histological damage score of the colon of DSS-treated mice with or without treatment with CONFMT or GLFMT. **f, g** Serum concentrations

of pro-inflammatory cytokines and relative protein expression levels of tight junction proteins in the colon of DSS-treated mice with/without treatment with CONFMT or GLFMT. **h–k** Principal coordinates analysis (PCoA) of weighted UniFrac distances, microbiota composition, and differential abundance of the fecal microbiota at the genus and specie levels as determined by RT-qPCR. Samples for western blot were derived from the same experiment and gels/blots were processed in parallel. One-way ANOVA with Tukey's test was used for statistical analysis of body weight and intestinal parameters, and the Kruskal-Wallis test and post-hoc Dunn's test was used for microbial analysis. Data were presented as mean  $\pm$  SEM. Source data were provided as a Source Data file.

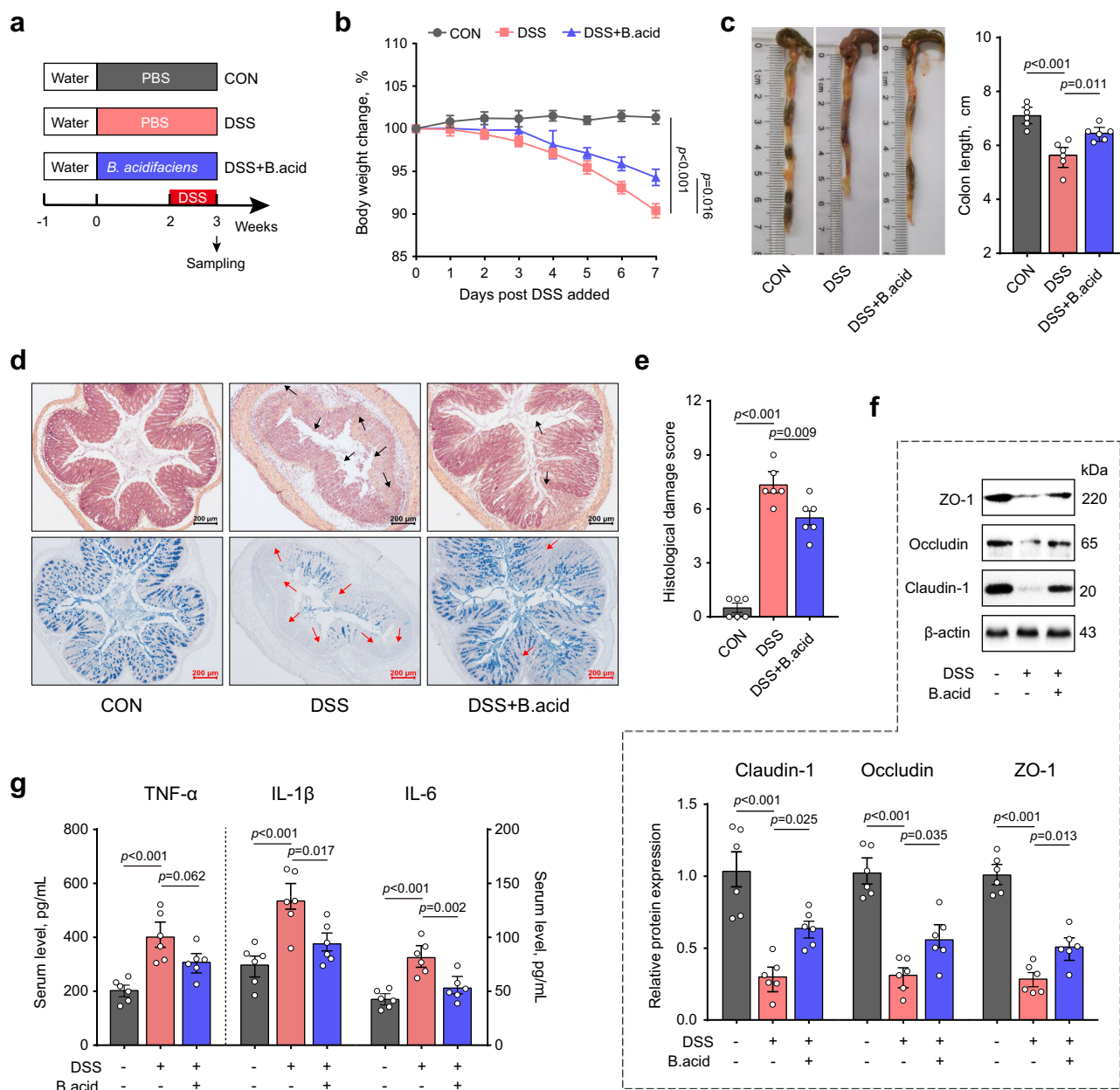


**Fig. 3 | *B. acidifaciens* protects against intestinal inflammation and barrier dysfunction.** After a week of acclimation, 8-week-old male C57BL/6J mice ( $n = 6$  per group) were subjected to daily oral gavage of PBS or  $2 \times 10^8$  CFU *B. acidifaciens* for three weeks. Colitis was induced in mice by providing 3% DSS in the third week. **a, b** Study design and body weight change in DSS-treated mice with/without *B. acidifaciens* treatment. **c–e** The length, H&E staining, Alcian blue staining, and histological damage score of the colon in DSS-treated mice with or without *B.*

*acidifaciens* treatment. **f, g** Relative protein expressions of tight junction proteins in the colon and serum concentrations of pro-inflammatory cytokines of DSS-treated mice with or without *B. acidifaciens* treatment. Samples for western blot were derived from the same experiment and gels/blots were processed in parallel. One-way ANOVA with Tukey's test was used for statistical analysis. Data were presented as mean  $\pm$  SEM. Source data were provided as a Source Data file.

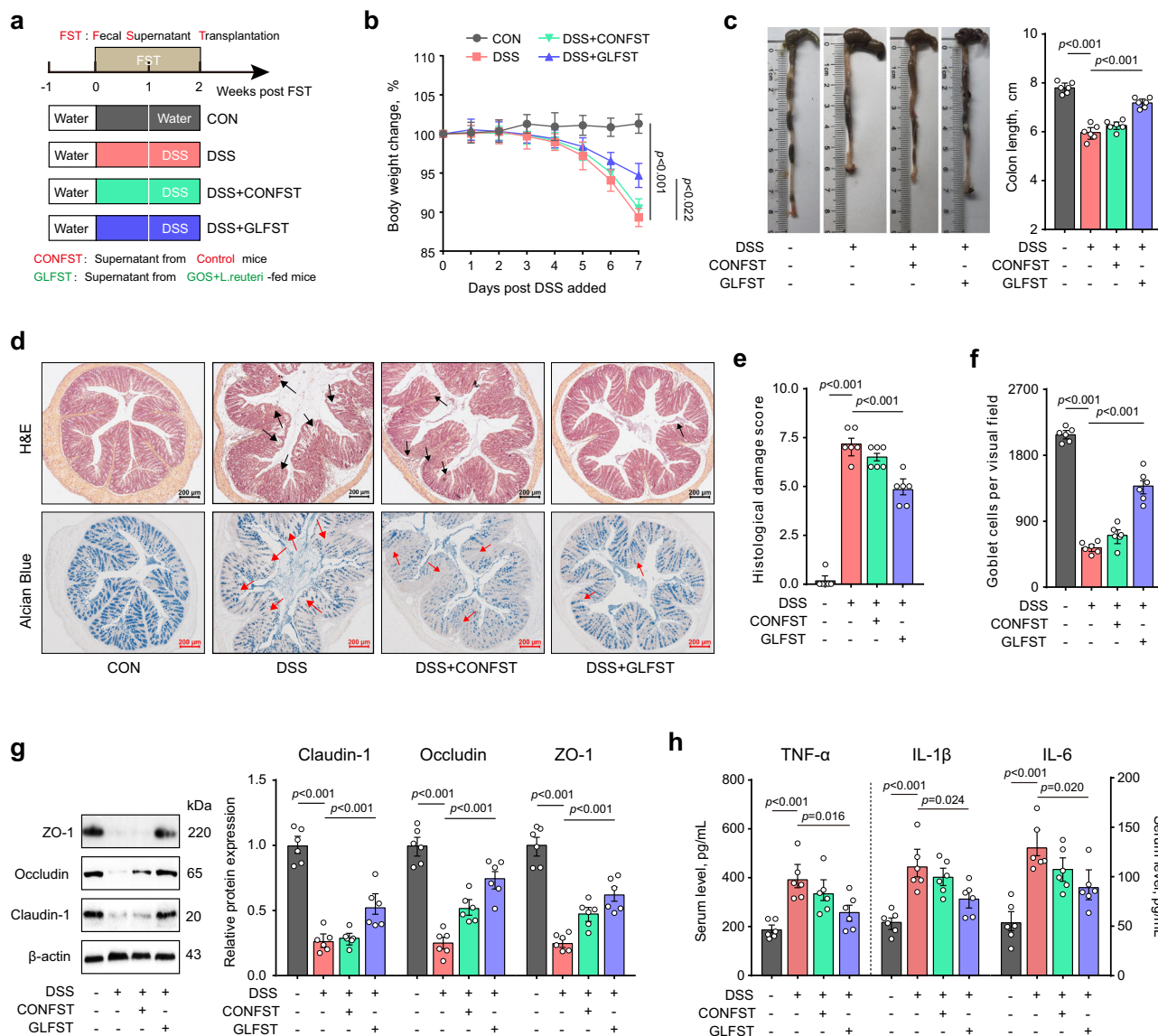


**Fig. 4 | Fecal supernatant of the symbiotic-supplemented mice alleviates the intestinal inflammation and barrier dysfunction.** After a week of acclimation, bacterial cell-free supernatant of the fecal microbiota was prepared from the mice fed standard chow (CONFST) or GOS/*L. reuteri* (GLFST) and orally administered to 8-week-old male C57BL/6J mice ( $n = 6$  per group) for two weeks. Colitis was induced in mice by providing 3% DSS in the second week. **a, b** Study design and body weight change in DSS-treated mice with/without treatment with CONFST or GLFST. **c–f** The length, H&E staining, Alcian blue staining, histological damage

score, and goblet cells number in the colon of DSS-treated mice with or without treatment with CONFST or GLFST. Relative protein expressions of tight junction proteins in the colon (**g**) and serum concentrations of pro-inflammatory cytokines (**h**) of DSS-treated mice with or without treatment with CONFST or GLFST. Samples for western blot were derived from the same experiment and gels/blots were processed in parallel. One-way ANOVA with Tukey's test was used for statistical analysis. Data were presented as mean  $\pm$  SEM. Source data were provided as a Source Data file.

observed between *B. acidifaciens* and C15:0 in LPS-challenged pigs (Fig. 9f).

To further validate our results, we retrieved and analyzed the C15:0 concentrations from several publicly available metabolomic datasets involving a total of 503 healthy controls and 649 UC patients from China, USA, Netherlands, and Norway in several recent studies<sup>12–16</sup>. Consistently, the C15:0 concentrations in the feces (Fig. 9g), serum (Fig. 9h), and colonic biopsy (Fig. 9i) of UC patients were significantly lower than those of healthy volunteers. Furthermore, compared to inactive UC patients, active UC patients showed significantly reduced C15:0 concentrations in the feces (Fig. 9j), serum (Fig. 9k), and colonic biopsy (Fig. 9l). These results collectively suggested that inflammation and barrier dysfunction correlate with diminished levels of *B. acidifaciens* and C15:0 across different intestinal inflammatory disease models in various animal species. Strategies such

as combining GOS and *L. reuteri* may hold therapeutic potential for UC. Additionally, administration of *B. acidifaciens* or C15:0 may also be promising for treating UC and other intestinal inflammatory disorders.

## Discussion

UC has emerged as a significant public health concern with a rising incidence<sup>1</sup>. Various factors, such as dysregulated immune response, dysbiosis, intestinal barrier dysfunction, have been implicated in UC pathogenesis<sup>17,18</sup>. Restoring homeostasis of the intestinal microbiota, inflammation, and barrier function is considered a primary therapeutic approach<sup>19,20</sup>. In this study, we demonstrated the protective effects and potential mechanisms of a synbiotic consisting of GOS and *L. reuteri* on intestinal inflammation and barrier dysfunction. We showed that this synbiotic improves intestinal health by enriching *B. acidifaciens*, which subsequently leads to increased synthesis of a key metabolite, C15:0.

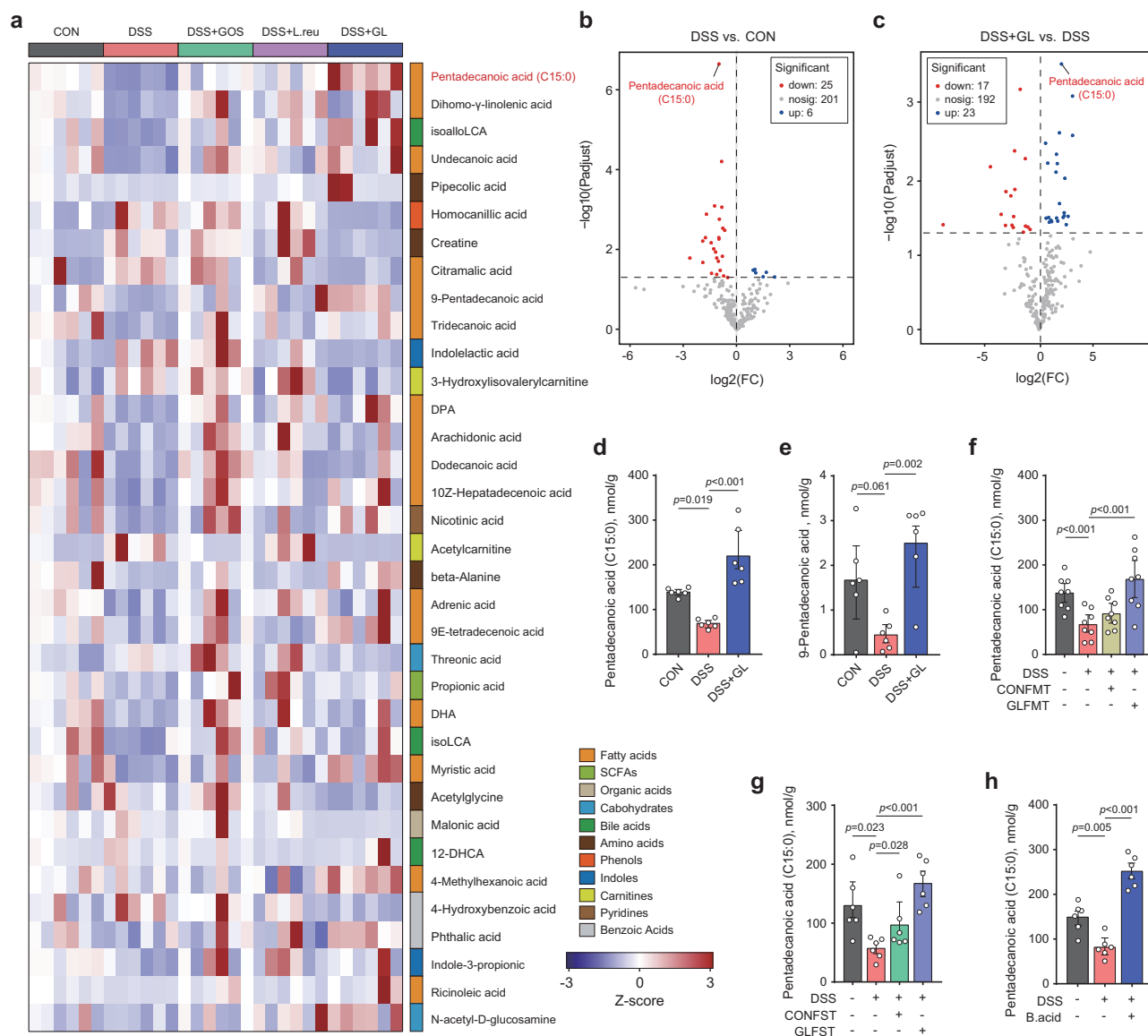


**Fig. 5 | Synbiotic GOS and *L. reuteri* enriches pentadecanoic acid (C15:0) in mice.** **a** Heatmap of differentially enriched metabolites in the feces of mice supplemented with GOS and *L. reuteri* individually or in combination ( $n = 6$  per group). **b, c** Volcano plot of differentially enriched metabolites among control, DSS and DSS + GL groups. **d, e** The fecal content of C15:0 or 9-pentadecanoic acid in DSS-treated mice with/without supplementation with the synbiotic GOS and *L. reuteri*

( $n = 6$  per group). **f-h** The fecal content of C15:0 in DSS-treated mice with/without oral administration of fecal microbiota (FMT,  $n = 8$  per group), Fecal cell-free supernatant (FST,  $n = 6$  per group), or *B. acidifaciens* ( $n = 6$  per group). One-way ANOVA with Tukey's test was used for statistical analysis. Data were presented as mean  $\pm$  SEM. Source data were provided as a Source Data file.

Intestinal health is improved due to the anti-inflammatory and barrier protective properties of *B. acidifaciens* and C15:0. These findings suggest that the synbiotic GOS and *L. reuteri*, along with *B. acidifaciens* and C15:0, holds promise as a dietary supplement for preventing UC development.

We further revealed UC patients, DSS-treated mice, and LPS-challenged pigs all exhibit a deficiency in *B. acidifaciens* and C15:0, underscoring the critical role of *B. acidifaciens* in UC development. *B. acidifaciens*, a dominant commensal bacterium in the intestine, has been reported to protect against liver injury and metabolic disorders<sup>21,22</sup>. Consistently, *B. acidifaciens* has been shown to elevate intestinal immunoglobulin A (IgA) levels and protect against pathogenic infections in IBD<sup>23</sup>. Alginate oligosaccharides were reported to improve immune function and dysbiosis by enriching *B. acidifaciens* in DSS-induced colitis<sup>24</sup>. Furthermore, extracellular vesicles of *B. acidifaciens* are capable of restoring mucosal barrier function and

microbiota balance in DSS-induced colitis<sup>25</sup>. These results confirmed the beneficial roles of *B. acidifaciens* in intestinal health, especially in UC.

Fatty acids play pivotal roles in the nutrition and protection of enterocytes while acting as mediators in transcriptional and inflammatory processes<sup>26,27</sup>. Previous studies have revealed alterations in the metabolism of long-chain fatty acids in the intestine of UC patients<sup>12,28,29</sup>. Consistently, our study found a significant reduction in C15:0, an odd-chain fatty acid, in UC patients, as well as in DSS-treated mice and LPS-challenged piglets. Studies with C15:0 have highlighted its anti-inflammatory, anti-fibrotic, and anticancer activities through various mechanisms, such as AMPK and PPAR- $\alpha/\delta$  activation, and inhibition of mTOR, JAK-STAT, and HDAC6 in vitro and in vivo<sup>30-35</sup>. We also revealed that C15:0 inhibits inflammatory response by suppressing the phosphorylation of NF- $\kappa$ B, which plays a central role in the homeostasis and activation of the immune system<sup>36-38</sup>.



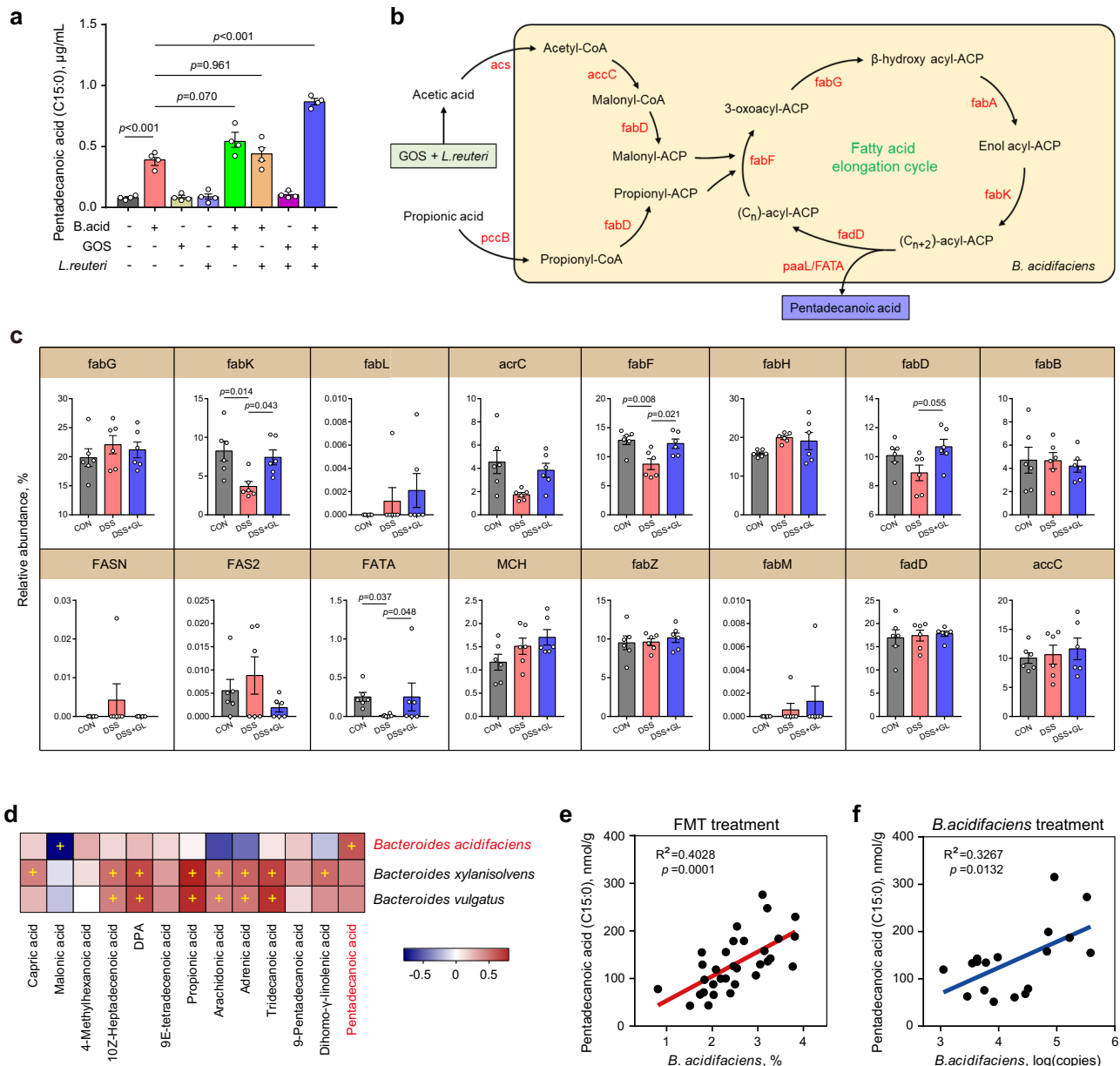


**Fig. 6 | *B. acidifaciens* synthesizes pentadecanoic acid (C15:0).** **a** Pentadecanoic acid concentrations in the supernatant of *B. acidifaciens* culture supplemented with or without GOS, *L. reuteri*, or their combination ( $n = 4$  per group). **b** Metabolic pathway of C15:0 in *B. acidifaciens*. **c** Relative abundances (%) of bacterial genes involved in C15:0 synthesis based on shotgun metagenomic analysis ( $n = 6$  per group). **d** Spearman two-tailed correlation analysis between *Bacteroides* spp. and representative fecal metabolites. **e, f** Linear regression analysis between fecal concentrations of C15:0 and relative abundance of *B. acidifaciens* in the feces of mice following transplantation with fecal microbiota (FMT,  $n = 8$  per group) or fecal bacterial cell-free supernatants (FST,  $n = 6$  per group). One-way ANOVA with Tukey's test was used for **(a)**, and Kruskal-Wallis test and post-hoc Dunn's test was

used for (e, f). Data were presented as mean  $\pm$  SEM. Source data were provided as a Source Data file. ACP acyl carrier protein, accC acetyl-CoA carboxylase, acrC enoyl-ACP reductase C, acs acetyl-CoA synthetase, FAS2 fatty acid synthase 2, FASN fatty acid synthase system, FATA fatty acyl-ACP thioesterase A, fabA 3-hydroxyacyl-ACP dehydratase, fabB 3-oxoacyl-ACP synthase I, fabD ACP-S-malonyltransferase, fabF 3-oxoacyl-ACP synthase II, fabG 3-oxoacyl-ACP reductase, fabH 3-oxoacyl-ACP synthase III, fabK enoyl-ACP reductase II, fabL enoyl-ACP reductase I, fabM trans-2-decenoyl-ACP isomerase, fabZ 3-hydroxyacyl-ACP dehydratase, fadD long-chain acyl-CoA synthetase, MCH medium chain hydrolase, paaL acyl-CoA thioesterase, pccB propionyl-CoA carboxylase beta chain.

Indeed, epidemiological studies have linked higher circulating C15:0 concentrations to lower cholesterol, triglycerides, liver enzymes, C-reactive protein, adipokines, body mass index, and improved insulin sensitivity and  $\beta$  cell function in humans<sup>39–45</sup>. Furthermore, C15:0 exhibits antimicrobial properties, inhibiting the growth of pathogenic bacteria and fungi<sup>46,47</sup>. Due to its role in the alleviation metabolic disorders and chronic inflammation, C15:0 has been proposed as a potential essential fatty acid<sup>31,39,44,48–50</sup>.

However, the mechanism by which C15:0 suppresses inflammation and NF- $\kappa$ B activation remains largely unknown. FATP4 is a major transporter and fatty acid CoA synthase mediating uptake and downstream biological activities of long-chain fatty acids<sup>[10,11]</sup>. Our study indicated that FATP4 was upregulated in DSS-treated mice following C15:0 supplementation. Binding and transporting of C15:0 to FATP4 ultimately led to the dephosphorylation of NF- $\kappa$ B p65, which reduced inflammation and improved barrier integrity. These findings align with

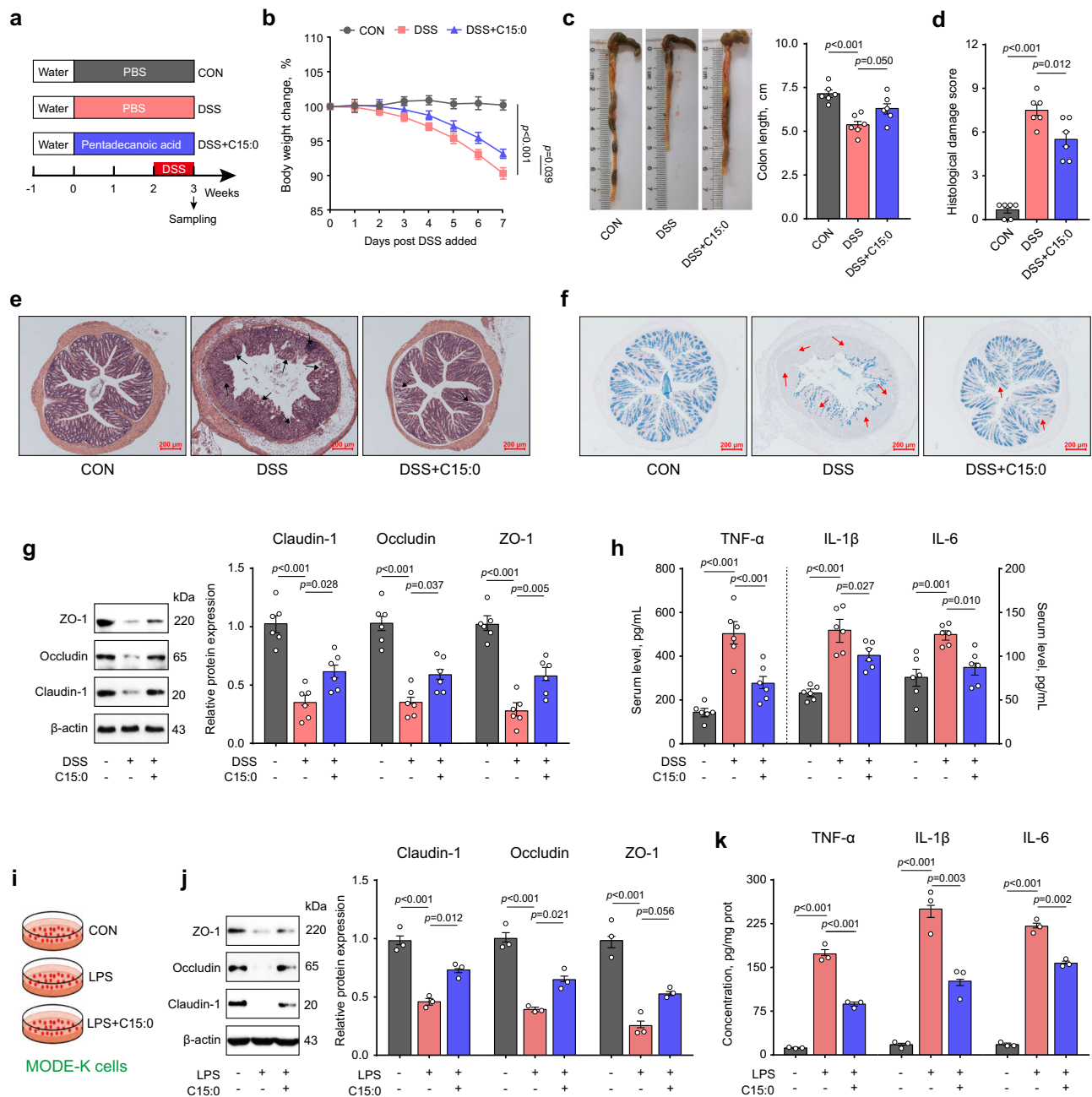


**Fig. 7 | Pentadecanoic acid (C15:0) promotes intestinal health by improving barrier function and suppressing inflammatory response.** After a week of acclimation, 8-week-old male C57BL/6J mice ( $n = 6$  per group) were subjected to daily oral gavage of PBS or 35 mg/kg C15:0 for three weeks. Colitis was induced in mice by providing 3% DSS in the final week. **a, b** Study design and body weight changes in DSS-treated mice with or without C15:0 treatment. **c–f** The length, histological damage score, H&E staining, and Alcian blue staining of the colon in DSS-treated mice with/without C15:0 treatment. **g, h** Relative protein expressions

of tight junction proteins in the colon and pro-inflammatory cytokines concentrations in the sera of DSS-treated mice with or without C15:0 treatment ( $n = 6$  per group). **i–k** Study design, relative protein expressions of tight junction proteins and concentrations of pro-inflammatory cytokines of LPS-treated MODE-K cells with or without C15:0 treatment ( $n = 3$  per group). Samples for western blot were derived from the same experiment and gels/blots were processed in parallel. One-way ANOVA with Tukey's test was used for statistical analysis. Data were presented as mean  $\pm$  SEM. Source data were provided as a Source Data file.

our observation that pharmacological blockage of FATP4 with a specific inhibitor reverses the anti-inflammatory and barrier protective properties of C15:0.

C15:0 was reported to be synthesized by microorganisms, such as *Yarrowia lipolytica*, *Rhodococcus*, and *Saccharomyces cerevisiae*<sup>51–54</sup>. A recent study showed that *Parabacteroides distasonis* also synthesizes C15:0 from inulin to ameliorate nonalcoholic steatohepatitis (NASH)<sup>55</sup>. In this study, we confirmed that *B. acidifaciens* produces C15:0 in response to GOS and *L. reuteri* both

in vitro and in vivo. For C15:0 synthesis, most current work focuses on the supplement of exogenous three-carbon compounds, like propionyl-CoA and malonyl-acyl carrier protein (ACP), as substrates<sup>56</sup>. In addition, the essential FAS enzymes for C15:0 synthesis were all encoded in the genome of *B. acidifaciens*, including  $\beta$ -ketoacyl-ACP synthase II (fabF),  $\beta$ -ketoacyl-ACP reductase (fabG),  $\beta$ -hydroxyacyl-ACP dehydratase (fabA), enoyl-ACP reductase (fabK), malonyl-CoA:ACP transacylase (fabD) and fatty acyl-CoA thioesterase (paal/FATA)<sup>51</sup>. Thus, *B. acidifaciens* may be

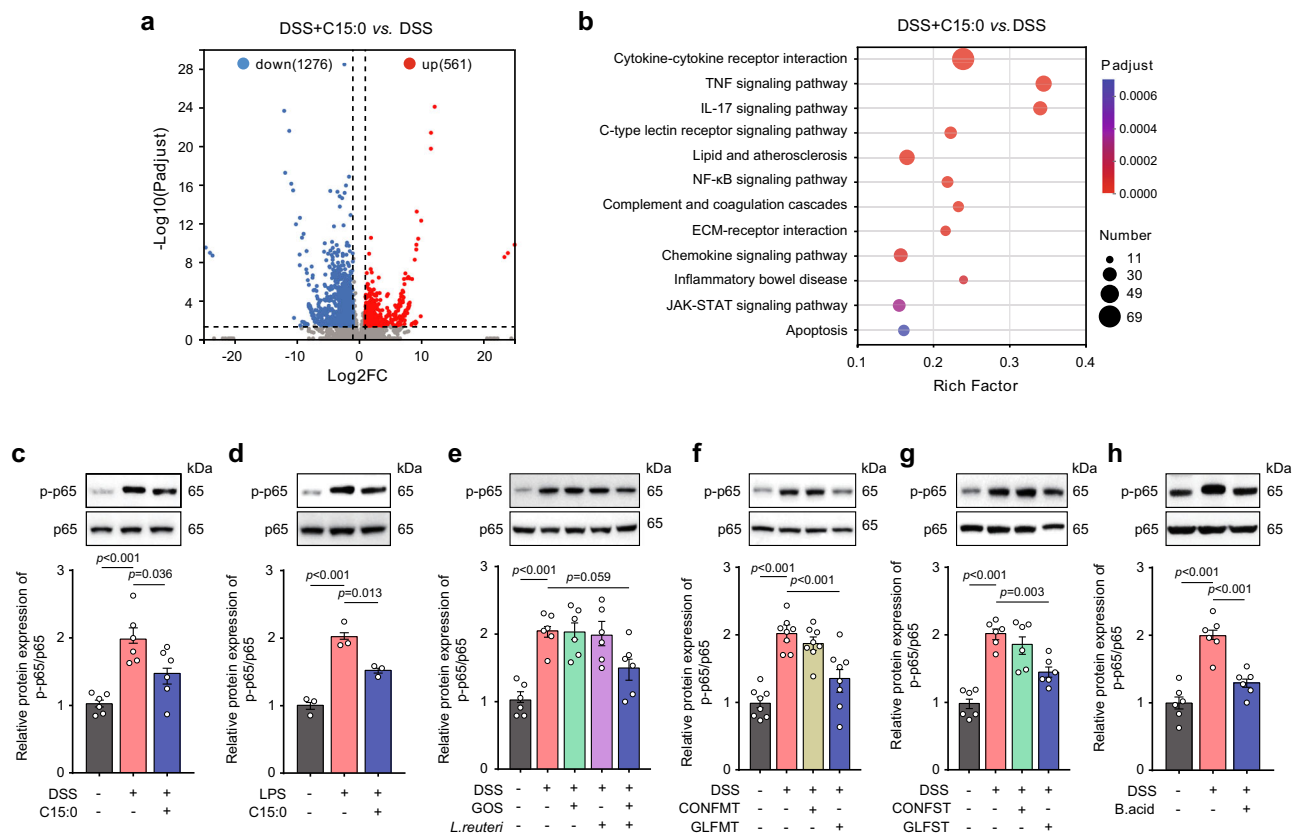


**Fig. 8 | *B. acidifaciens*-derived pentadecanoic acid (C15:0) suppresses NF-κB activation.** **a, b** Volcano plot and KEGG pathways of differentially expressed genes in the colonic segments of DSS-treated mice with or without oral administration of C15:0. **c, d** Phosphorylation of NF-κB p65 in the colon of DSS-treated mice ( $n = 6$  per group) or LPS-challenged MODE-K cells ( $n = 3$  per group) with or without treatment of C15:0. **e–h** Phosphorylation of NF-κB p65 in the colon of DSS-treated mice in

response to synbiotic (GOS and/or *L. reuteri*,  $n = 6$  per group), fecal microbiota transplantation (FMT,  $n = 8$  per group), fecal bacterial cell-free supernatant (FST,  $n = 6$  per group), or *B. acidifaciens* ( $n = 6$  per group). One-way ANOVA with Tukey's test was used for (**c–h**). The samples in each separate were derived from the same experiment and gels/blots were processed in parallel. Data were presented as mean  $\pm$  SEM. Source data were provided as a Source Data file.

genetically enhanced for industrial production of C15:0, similar to a recent metabolic engineering attempt with *E. coli*<sup>57</sup>.

It is noted that anti-tumor necrosis factor (TNF) agents, thiopurines, and glucocorticoids are standard treatments for UC patients, reducing the disease activity index (DAI) by approximately 50%<sup>58–60</sup>. In our study, supplementation with the synbiotic (GOS and *L. reuteri*), *B. acidifaciens*, or C15:0 significantly reduced colonic damage by 25–30%, as indicated by a lower histological damage score in DSS-induced colitis. Although the effect size of our nutritional strategies appears smaller than current UC treatments, further optimizations, such as microencapsulation, dosage adjustments, and screening for more effective bacterial strains, will undoubtedly enhance their efficacy against UC.

Collectively, our findings demonstrate that a synbiotic combination of GOS and *L. reuteri* protects against intestinal inflammation and barrier dysfunction by promoting the synthesis of pentadecanoic acid (C15:0) from *B. acidifaciens*. This critical link between synbiotics, commensal bacteria, and bacterial metabolites provides evidence and potential therapeutic avenues for UC and other intestinal inflammatory disorders.

## Methods

### Ethical statement

The clinical cohort was approved by the Ethics Committee of Jiangyin People's Hospital Affiliated to Nantong University (Jiangsu, China) and followed the Declaration of Helsinki under the protocol number of 2023–043. All animal experiments were approved by the Animal Care and Use Committee of China Agricultural University (Beijing, China) under the protocol number of Aw60213202-1-1.

### Human clinical patient data and sample collection

Included in this study were 15 healthy donors (4 females and 11 males) and 11 UC patients (5 females and 6 males) aged from 25 to 70, which were patients admitted to Jiangyin People's Hospital affiliated with Nantong University (Jiangsu, China) in 2023. The characteristics of the study participants were detailed in Supplementary Table S1. UC patients were diagnosed based on clinical, endoscopic, and surgical specimens. Healthy donors and acute UC patients were free from antibiotics for more than two weeks prior to fecal collection. Informed consent was obtained from all participants. The samples were stored at  $-80^{\circ}\text{C}$  for further analysis. Additionally, to further validate our results, the C15:0 concentrations were retrieved and reanalyzed from publicly available metabolomic datasets involving a total of 503 healthy controls and 649 UC patients from China, USA, Netherlands, and Norway<sup>12–16</sup>. Detailed patient information was provided in Supplementary Table S2.

### Animal experiments

In the mouse model of DSS-induced colitis, 6- to 8-week-old male C57BL/6J mice were housed in a specific pathogen-free facility under ambient temperature of  $20–22^{\circ}\text{C}$ , humidity of 40–60%, and 12-h light/12-h dark cycle with free access to water and standard chow. The composition of the chow diet including: cornstarch (46.57%), maltodextrin (15.50%), casein (14.00%), sucrose (10.00%), cellulose fibers (5.00%), soy oil (4.00%), mineral mix (3.50%), vitamin mix (1.00%), L-cysteine (0.18%), and choline (0.25%). To induce colitis, DSS (Coolaber, Beijing, China) was added to drinking water to the final concentration of 3% for a week. To administer GOS, *L. reuteri* or the

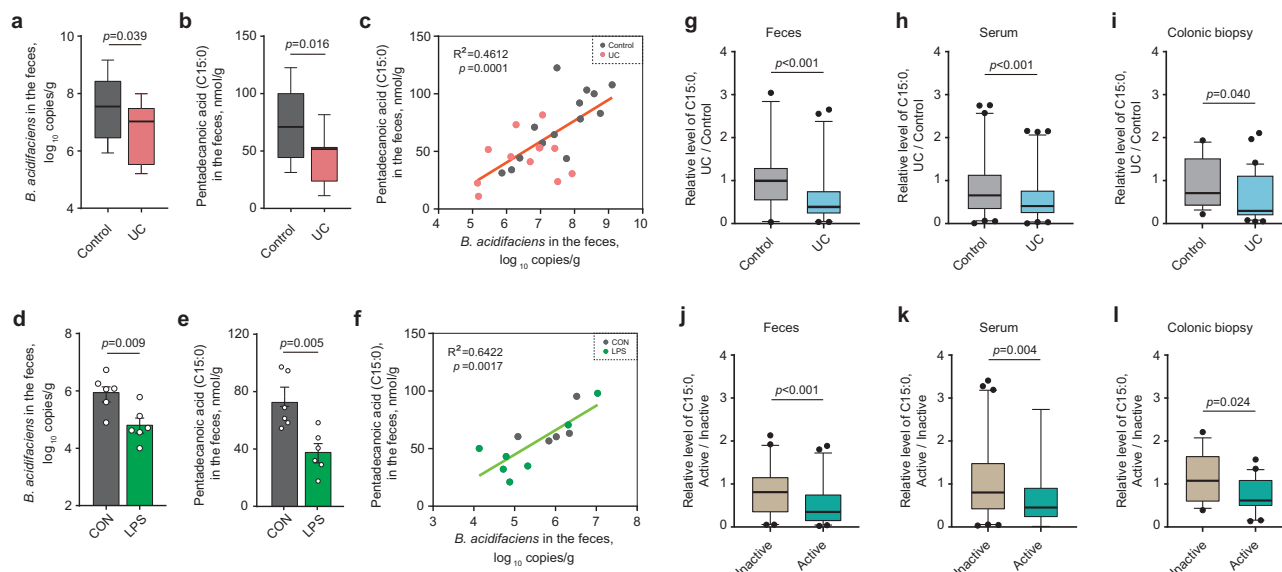


**Fig. 9 | *B. acidifaciens* and pentadecanoic acid (C15:0) are downregulated in UC patients and LPS-challenged piglets.** **a–c** Relative abundances of *B. acidifaciens*, the C15:0 concentrations, and their correlation in the feces of healthy volunteers ( $n = 15$ ) and UC patients ( $n = 11$ ) admitted to Jiangyin People's Hospital affiliated with Nantong University (Jiangsu, China) in 2023. **d–f** Relative abundance of *B. acidifaciens* ( $n = 6$  per group), the C15:0 concentrations ( $n = 6$  per group), and their correlation in the feces of piglets with and without LPS challenge. **g–i** Several publicly available metabolomic datasets from China, USA, Netherlands, and Norway were reanalyzed, showing the concentrations of C15:0 in the feces, serum, and colonic biopsy of healthy controls ( $n = 503$ ) and UC patients ( $n = 649$ ). **j–l** Active

and inactive UC patients were further selected from the same large metabolomic datasets and analyzed for relative concentrations of C15:0 in the feces, serum, and colonic biopsy of inactive UC ( $n = 408$ ) and active UC ( $n = 167$ ) patients. The box-plot (**a, b, g–l**) displays the distribution of concentrations for each metabolite, with the box representing the interquartile range (5th to 95th percentiles), the center line representing the median, and the whiskers representing the minimum and maximum values. Unpaired two-tailed Student's *t* test was used for (**d, e**), and two-sided Mann-Whitney *U* test was used for (**a, b, g–l**). Spearman's two-tailed correlation was used for (**c, f**). Data were presented as mean  $\pm$  SEM. Source data were provided as a Source Data file.

synbiotic, GOS (5% w/w; Coolaber) was supplemented to the diet for four weeks with or without daily oral gavage of  $2 \times 10^8$  CFU *L. reuteri* (BNCC 186135, BeNa Culture Collection, China). GOS (5% w/w; Coolaber) was also supplemented to the diet of DSS-treated mice for three weeks with or without daily oral gavage of  $2 \times 10^8$  CFU of two other *L. reuteri* strains (#1 and #2, isolated from mouse feces in our lab). For fecal microbiota transplantation (FMT), a cocktail of antibiotics (1 g/L streptomycin, 0.5 g/L ampicillin, 0.5 g/L vancomycin, and 1 g/L gentamicin) were added to drinking water for 4 weeks to deplete the intestinal microbiota. Mice were then orally administered with 0.2 mL PBS or fecal suspension daily for two weeks. The fecal suspension was obtained from the mice fed standard chow or administered with GOS and *L. reuteri*, followed by suspension of 100 mg feces in 1.5 mL sterile anaerobic PBS. Oral administration of *B. acidifaciens* (BNCC 353574, BeNa Culture Collection, China) or *B. acidifaciens* JCM10556 (DSMZ, Germany) was performed by gavaging  $2 \times 10^8$  CFU of the bacteria in 0.2 mL PBS daily for three weeks. For fecal supernatant transplantation (FST), mice were orally administered with 0.2 mL PBS or fecal bacterial cell-free supernatant daily for two weeks. The bacterial cell-free supernatant was obtained from the feces of mice fed standard chow or administered with GOS and *L. reuteri*, followed by centrifugation at  $8000 \times g$  for 5 min and filtration through a 0.22  $\mu$ m filter. Oral administration of pentadecanoic acid (C15:0, 35 mg/kg)<sup>31</sup> was performed by gavaging in 0.2 mL PBS daily for three weeks.

For sampling, a colonic segment was collected from each mouse and fixed in 4% paraformaldehyde for H&E staining and/or Alcian blue (AB) staining. Histological scoring was performed with each segment on Zeiss Axio Imager microscope based on the extent of epithelial surface loss, crypt destruction, and inflammatory cell infiltration as previously described<sup>61</sup>. The acidic goblet cells were counted with Image J software<sup>62</sup>. Feces and the remaining colonic segments were collected and stored at  $-80^\circ\text{C}$  for further analysis.

In the pig model of LPS-induced intestinal inflammation, twelve 24-day-old male weaned Duroc-Landrace-Yorkshire piglets were housed in an environmentally controlled room at  $22\text{--}25^\circ\text{C}$  with free access to feed and water. The composition of diet for weaned piglets including: corn (58.60%), soybean meal (13.00%), whey powder (8.00%), fish meal (3.00%), soy protein concentrate (5.00%), extruded full-fat soybean (5.00%), glucose (2.00%), soybean oil (2.00%), CaHPO<sub>4</sub> (1.00%), limestone (0.80%), NaCl (0.20%), L-lysine-HCl (0.55%), DL-methionine (0.10%), L-threonine (0.20%), L-tryptophan (0.05%), mineral and vitamin premix (0.50%). Piglets were administered intraperitoneally with 3 mL sterile saline in the presence or absence of LPS (100  $\mu$ g/kg BW; Sigma-Aldrich) 6 h prior to samples collection.

#### DNA extraction and 16S rRNA gene sequencing and analysis

Total genomic DNA of fecal samples were extracted for the amplification using universal primers 338 F/806 R targeting the V3-V4 region of the bacterial 16S rRNA gene and sequenced on Illumina MiSeq platform. Data analysis was performed on the free online platform of Majorbio Cloud Platform ([www.majorbio.com](http://www.majorbio.com)). In brief, raw paired-end reads were strictly analyzed using QIIME 2<sup>63</sup>. Taxonomic assignment was achieved using RDP classifier and annotated with the SILVA138 reference database. Principal coordinates analysis (PCoA) was based on unweighted Unifrac distances. Differentially enriched bacteria taxa were based on Kruskal-Wallis test and post-hoc Dunn's test. Spearman rank correlation coefficient and linear regression were used for correlation analysis.

#### Shotgun metagenomic sequencing and analysis

Total genomic DNA was used for sequencing and library construction on Illumina NovaSeq platform. Data analysis was performed on the free online platform of Majorbio Cloud Platform ([www.majorbio.com](http://www.majorbio.com)). In brief, raw reads were filtered using Fastp and assembled using MEGAHIT, and the assembled contig was predicted using



MetaGene<sup>64,65</sup>. After a non-redundant gene catalog was constructed using CD-HIT, gene abundance with 95% identity was calculated using SOAPaligner<sup>66,67</sup>. Representative sequences were aligned to NR database for taxonomic annotations using Diamond<sup>68</sup>. Differential analysis was achieved using Kruskal-Wallis test and post-hoc Dunn's test. The top 20 species were selected as variables in the random forest model.

### Quantification of specific bacterial species

After total genomic DNA was extracted as mentioned above, RT-qPCR was conducted using SYBR Premix Ex Taq™ II kit (Takara) on a Light Cycler® System (Roche). Specific primers for total bacteria and specific bacterial species were synthesized by Sangon Biotech (Shanghai) Co., Ltd. (China) and shown in Supplementary Table S3. Standard curves were obtained by constructing standard plasmids containing 16S rRNA genes. The copy numbers of each target specific bacterial species were calculated using the corresponding standard curves. The gene copy numbers were calculated using the following equation: [DNA concentration (mg/mL) × 6.0233 × 10<sup>23</sup> copies/mol] / [DNA size (bp) × 660 × 10<sup>6</sup>]. Each sample was done in duplicate and average before further analysis. The relative abundance of target specific bacterial species was the copy number ratio of individual specific bacterial species to total bacteria.

### Whole-genome sequencing and analysis

Total genomic DNA was extracted from *B. acidifaciens*, and sequencing libraries were prepared for Illumina and PacBio sequencing platforms and sequenced by Shanghai Majorbio Bio-pharm Technology (Shanghai, China) at the 100 × coverage. Raw reads were quality trimmed with Fastp and assembled with Unicycler<sup>69</sup>. Genomic sequences of *B. acidifaciens* were classified and annotated using eggNOG and KEGG databases. The genome-scale metabolic modeling was constructed with MetaCyc pathways<sup>70</sup>.

### Metabolomic profiling and analysis

Targeted metabolomics profiling was conducted using Q300 Metabolite Array from Metabo-Profile Biotechnology (Shanghai, China). Briefly, 5 mg feces were homogenized in 25 µL water, and the metabolites were extracted with 120 µL ice-cold methanol containing 306 internal standards representing more than 11 classes of metabolites, such as amino acids, bile acids, fatty acids, organic acids, carbohydrates, phenols, indoles, carnitines, pyridines, and benzoic acids. Following centrifugation at 18,000 × g for 20 min, 20 µL supernatant was derivatized with prepared derivative reagents on Eppendorf epMotion Workstation. UPLC-MS/MS system was used to quantitate targeted metabolites by comparing with internal standards. Metabolite identification was based on Metabo-Profile LIMS system<sup>71</sup>. Raw data files generated from UPLC-MS/MS were processed using the TMBQ software for integration, calibration, and quantitation of each metabolite. The statistical analysis was performed on Metabo-Profile iMAP platform<sup>72</sup>. Differentially enriched metabolites were identified using Wilcoxon rank-sum test, and adjusted  $P < 0.05$  was deemed significant. Z-scores were calculated after Log<sub>2</sub> transformations of relative abundances of individual metabolites. Heatmaps and volcano plots were generated using Complex Heatmap and ggplot in R language, respectively<sup>55</sup>.

### Bacterial culture and pentadecanoic acid biosynthesis in vitro

*L. reuteri* (BNCC 186135) and two *L. reuteri* strains (#1 and #2) isolated in the mouse feces by our lab were cultured anaerobically in MRS medium, while *B. acidifaciens* (BNCC 353574 and JCM10556) were cultured anaerobically in BHI medium at 37°C. The culture medium used for in vitro pentadecanoic acid biosynthesis is comprised of casitone (10.00 g/L), yeast extract (2.50 g/L), MgSO<sub>4</sub>·7H<sub>2</sub>O (45.00 mg/L), CaCl<sub>2</sub>·2H<sub>2</sub>O (90.00 mg/L), M9 salt (11.28 g/L), L-cysteine HCl (0.50 g/L), haemin (5.00 mg/L), and vitamin K (0.50 mg/L). GOS (1%, w/v), *L.*

*reuteri* (10<sup>8</sup> CFU/mL, 1%, v/v) or GL-derived fecal supernatant (1%, v/v) was added when needed.

### Mouse cecum microbiota cultivation and *B. acidifaciens* detection

After 8-week-old male C57BL/6J mice euthanized, the caecum was removed aseptically and its content (portions of about 100 µL) was transferred under CO<sub>2</sub> flushing to PYG medium (Modified), including: trypticase peptone (5.00 g/L), peptone (5.00 g/L), yeast extract (10.00 g/L), beef extract (5.00 g/L), glucose (5.00 g/L), K<sub>2</sub>HPO<sub>4</sub> (2.04 g/L), Tween 80 (1.00 mL/L), CaCl<sub>2</sub>·2H<sub>2</sub>O (10.00 mg/L), MgSO<sub>4</sub>·7H<sub>2</sub>O (20.00 mg/L), KH<sub>2</sub>PO<sub>4</sub> (40.00 mg/L), NaHCO<sub>3</sub> (0.40 g/L), NaCl (80.00 mg/L), resazurin (1.00 mg/L), vitamin K1 (1.00 µL/L), haemin (5.00 mg/L), L-cysteine-HCl (0.50 g/L), and distilled water (0.95 L)<sup>73</sup>. For *B. acidifaciens* enriching experiment, GOS (1 mM), *L. reuteri* (10<sup>6</sup> CFU/mL) or their combination, as well as beta-alanine (1 mM), N-acetyl-D-glucosamine (1 mM), 4-methylhexanoic acid (1 mM) or myristic acid (1 mM) was supplemented in the culture medium. The relative abundance of *B. acidifaciens* in the culture medium was detected by RT-qPCR with specific primer as described above.

### Cells culture and treatment

Human Caco-2 cells and murine MODE-K cells were cultured in DMEM/F12 medium supplemented with 10% FBS, 100 U/mL penicillin, and 100 µg/mL streptomycin at 37°C and 5% CO<sub>2</sub>. After treated with/without 10 µg/mL LPS, and/or 50 µM C15:0, and/or 1 µM dihydropyrimidinone (DHPM, Sigma) for 24 h, cells were harvested for further analysis.

### RNA extraction, reverse transcription, and RT-qPCR

Total RNA was extracted using TRIzol reagent (Invitrogen, USA) according to the manufacturer's instructions. Reverse transcription was performed in duplicate using Prime Script™ RT Kit (Takara, Japan), and qPCR was conducted using SYBR Premix Ex Taq™ II kit (Takara, Japan) on a Light Cycler® System (Roche, USA). Primers for RT-qPCR were synthesized by Sangon Biotech (Shanghai) Co., Ltd. (China), and shown in Supplementary Table S3. The relative gene expressions were calculated using the 2<sup>-ΔΔCt</sup> method using β-actin as the reference gene.

### RNA-seq and data analysis

RNA-seq of total RNA samples was performed on Illumina HiSeq X Ten platform. The raw paired end reads were trimmed and quality controlled by Fastp, and then aligned to *Mus musculus* reference genome (GRCm39)<sup>74</sup>. Data analysis was performed on free online platform of Majorbio Cloud Platform ([www.majorbio.com](http://www.majorbio.com)). Differentially expressed genes were identified through pairwise comparisons using DESeq2 with |log<sub>2</sub>FC| > 1 and  $q < 0.05$ . KEGG analysis was performed at  $q < 0.05$  using Goatools and KOBAS<sup>75</sup>. Differential expression of selected genes were further validated with RT-qPCR. The primers were synthesized by Sangon Biotech (Shanghai) Co., Ltd. (China) and shown in Supplementary Table S3.

### Protein extraction, quantification, and western blot

Proteins were extracted with RIPA buffer consisting of 50 mM Tris (pH 7.4), 150 mM NaCl, 1% Triton X-100, 1% sodium deoxycholate, 0.1% SDS, 2 mM sodium pyrophosphate, 25 mM β-glycerophosphate, 1 mM EDTA, 1 mM Na<sub>3</sub>VO<sub>4</sub>, 0.5 µg/mL leupeptin, protease inhibitors, and phosphatase inhibitors. Extracted proteins were quantified with the BCA method. Western blot was performed with the following antibodies: β-actin (Sigma-Aldrich, A5441, 1:1,000), Claudin-1 (Invitrogen, 2H10D10, 1:1,000), Occludin (Abcam, ab216327, 1:1,000), ZO-1 (Abcam, ab221547, 1:1,000), NF-κB p65 (Cell Signaling Technology, 8242, 1:1,000), p-NF-κB p65 (Cell Signaling Technology, 3033, 1:1,000), FATP4 (Proteintech, 11013-1-AP, 1:500), and HRP-conjugated

secondary antibody (Cell Signaling Technology, 91196, 1:10,000). After stripes collection, the signals were quantified using Image J software<sup>76</sup>. The uncropped and unprocessed scans have been supplied in the Source Data file.

### Statistics & reproducibility

No statistical methods were used to predetermine sample size for in vivo and in vitro experiments, but at least three samples were used per experimental group and condition. Samples and experimental animals were randomly assigned to experimental groups. The investigators were blinded to allocation during experiments and outcome assessment.

Data were analyzed using SPSS 20.0 (IBM, United States). No data were excluded from the analysis. The Shapiro-Wilk test was performed to assess the normality of each dataset. If  $p > 0.05$ , the data was deemed normally distributed, and two-tailed Student's *t* test was used to detect statistical significance for two groups, while one-way ANOVA with Tukey's test was used for more than two groups. If  $p < 0.05$ , the two-tailed Mann-Whitney U test was used to detect statistical significance for two groups and the Kruskal-Wallis test and post-hoc Dunn's test for more than two groups.

### Reporting summary

Further information on research design is available in the Nature Portfolio Reporting Summary linked to this article.

### Data availability

The metagenomic sequencing data, 16S rRNA sequencing data, whole-genome sequencing data, and RNA-seq data were available in the NCBI SRA database under the accession numbers [PRJNA1048359](#) and [PRJNA1154812](#). The output of the metabolomics data and all other data generated during this study were available in Source Data provided with this paper. Source data are provided with this paper.

### Code availability

All analyses were conducted using open-source software, which has been explicitly stated in the method section. No custom code or mathematical algorithm was utilized in this study.

### References

- Kobayashi, T. et al. Ulcerative colitis. *Nat. Rev. Dis. Primers* **6**, 74 (2020).
- Zhang, Y. Z. & Li, Y. Y. Inflammatory bowel disease: pathogenesis. *World J. Gastroenterol.* **20**, 91–99 (2014).
- Andersen, A. D. et al. Synbiotics combined with glutamine stimulate brain development and the immune system in preterm pigs. *J. Nutr.* **149**, 36–45 (2019).
- Kolida, S. & Gibson, G. R. Synbiotics in health and disease. *Annu. Rev. Food Sci. Technol.* **2**, 373–393 (2011).
- Ma, L. et al. Anti-Inflammatory Effect of clostridium butyricum-derived extracellular vesicles in Ulcerative Colitis: Impact on host microRNAs expressions and gut microbiome profiles. *Mol. Nutr. Food Res.* **67**, e2200884 (2023).
- Mu, Q., Tavella, V. J. & Luo, X. M. Role of *Lactobacillus reuteri* in human health and diseases. *Front. Microbiol.* **9**, 757 (2018).
- Wang, J., Tian, S., Yu, H., Wang, J. & Zhu, W. Response of colonic mucosa-associated microbiota composition, mucosal immune homeostasis, and barrier function to early life galactooligosaccharides intervention in suckling piglets. *J. Agric. Food Chem.* **67**, 578–588 (2019).
- Wu, Y. et al. Strain specificity of lactobacilli with promoted colonization by galactooligosaccharides administration in protecting intestinal barriers during *Salmonella* infection. *J. Adv. Res.* **56**, 1–14 (2024).
- Rattanaprasert, M. et al. Genes involved in galactooligosaccharide metabolism in *Lactobacillus reuteri* and their ecological role in the gastrointestinal tract. *Appl. Environ. Microb.* **85**, e01788–01719 (2019).
- Li, Z., Liu, H., Xu, B. & Wang, Y. Enterotoxigenic *Escherichia coli* interferes FATP4-dependent long-chain fatty acid uptake of intestinal epithelial enterocytes via phosphorylation of ERK1/2-PPAR $\gamma$  pathway. *Front. Physiol.* **10**, 798 (2019).
- Lin, M. H. et al. Fatty acid transport protein 4 is required for incorporation of saturated ultralong-chain fatty acids into epidermal ceramides and monoacylglycerols. *Sci. Rep.* **9**, 13254 (2019).
- Franzosa, E. A. et al. Gut microbiome structure and metabolic activity in inflammatory bowel disease. *Nat. Microbiol.* **4**, 293–305 (2018).
- Weng, Y. J. et al. Correlation of diet, microbiota and metabolite networks in inflammatory bowel disease. *J. Dig. Dis.* **20**, 447–459 (2019).
- Lloyd-Price, J. et al. Multi-omics of the gut microbial ecosystem in inflammatory bowel diseases. *Nature* **569**, 655–662 (2019).
- Di'Narzo, A. F. et al. Integrative analysis of the inflammatory bowel disease serum metabolome improves our understanding of genetic etiology and points to novel putative therapeutic targets. *Gastroenterology* **162**, 828–843.e811 (2022).
- Diab, J. et al. Lipidomics in Ulcerative Colitis reveal alteration in mucosal lipid composition associated with the disease state. *Inflamm. Bowel Dis.* **25**, 1780–1787 (2019).
- Camilleri, M., Madsen, K., Spiller, R., van Meerveld, B. G. & Verne, G. N. Intestinal barrier function in health and gastrointestinal disease. *Neurogastroenterol. Motil.* **24**, 503–512 (2012).
- Salim, S. Y. & Soderholm, J. D. Importance of disrupted intestinal barrier in inflammatory bowel diseases. *Inflamm. Bowel Dis.* **17**, 362–381 (2011).
- Birchenough, G. & Hansson, G. C. Bacteria tell us how to protect our intestine. *Cell Host Microbe* **22**, 3–4 (2017).
- Fan, L. et al. Gut microbiota bridges dietary nutrients and host immunity. *Sci. China Life Sci.* **66**, 2466–2514 (2023).
- Yang, J. Y. et al. Gut commensal *Bacteroides acidifaciens* prevents obesity and improves insulin sensitivity in mice. *Mucosal Immunol.* **10**, 104–116 (2017).
- Wang, H. et al. *Bacteroides acidifaciens* in the gut plays a protective role against CD95-mediated liver injury. *Gut Microbes* **14**, 2027853 (2022).
- Nakajima, A. et al. A soluble fiber diet increases *Bacteroides fragilis* group abundance and immunoglobulin A production in the gut. *Appl. Environ. Microbiol.* **86**, e00405–e00420 (2020).
- Peng, J. et al. *Saffron petal*, an edible byproduct of *Saffron*, alleviates dextran sulfate sodium-induced colitis by inhibiting macrophage activation and regulating gut microbiota. *J. Agric. Food Chem.* **71**, 10616–10628 (2023).
- Zheng, C. et al. *Bacteroides acidifaciens* and its derived extracellular vesicles improve DSS-induced colitis. *Front. Microbiol.* **14**, 1304232 (2023).
- Yan, D. et al. Fatty acids and lipid mediators in inflammatory bowel disease: From mechanism to treatment. *Front. Immunol.* **14**, 1286667 (2023).
- Brown, E. M., Clardy, J. & Xavier, R. J. Gut microbiome lipid metabolism and its impact on host physiology. *Cell Host Microbe* **31**, 173–186 (2023).
- Heimerl, S. et al. Alterations in intestinal fatty acid metabolism in inflammatory bowel disease. *Biochim. Biophys. Acta* **1762**, 341–350 (2006).
- Ma, C., Vasu, R. & Zhang, H. The role of long-chain fatty acids in inflammatory bowel disease. *Mediators Inflamm.* **2019**, 8495913 (2019).

30. Ediriweera, M. K., To, N. B., Lim, Y. & Cho, S. K. Odd-chain fatty acids as novel histone deacetylase 6 (HDAC6) inhibitors. *Biochimie* **186**, 147–156 (2021).
31. Venn-Watson, S., Lumpkin, R. & Dennis, E. A. Efficacy of dietary odd-chain saturated fatty acid pentadecanoic acid parallels broad associated health benefits in humans: Could it be essential? *Sci. Rep.* **10**, 8161 (2020).
32. Fu, W. et al. Pentadecanoic acid promotes basal and insulin-stimulated glucose uptake in C2C12 myotubes. *Food Nutr. Res.* **65**, 4527 (2021).
33. To, N. B., Truong, V. N., Ediriweera, M. K. & Cho, S. K. Effects of combined pentadecanoic acid and tamoxifen treatment on tamoxifen resistance in MCF-7/SC breast cancer cells. *Int. J. Mol. Sci.* **23**, 11340 (2022).
34. Venn-Watson, S. K. & Butterworth, C. N. Broader and safer clinically-relevant activities of pentadecanoic acid compared to omega-3: Evaluation of an emerging essential fatty acid across twelve primary human cell-based disease systems. *PLoS One* **17**, e0268778 (2022).
35. To, N. B., Nguyen, Y. T., Moon, J. Y., Ediriweera, M. K. & Cho, S. K. Pentadecanoic acid, an odd-chain fatty acid, suppresses the stemness of MCF-7/SC human breast cancer stem-like cells through JAK2/STAT3 signaling. *Nutrients* **12**, 1663 (2020).
36. Christian, F., Smith, E. L. & Carmody, R. J. The regulation of NF- $\kappa$ B subunits by phosphorylation. *Cells* **5**, 12 (2016).
37. Park, M. H. & Hong, J. T. Roles of NF- $\kappa$ B in cancer and inflammatory diseases and their therapeutic approaches. *Cells* **5**, 15 (2016).
38. Taniguchi, K. & Karin, M. NF- $\kappa$ B, inflammation, immunity and cancer: coming of age. *Nat. Rev. Immunol.* **18**, 309–324 (2018).
39. Prada, M. et al. Association of the odd-chain fatty acid content in lipid groups with type 2 diabetes risk: A targeted analysis of lipidomics data in the EPIC-Potsdam cohort. *Clin. Nutr.* **40**, 4988–4999 (2021).
40. Polonskaya, Y. V. et al. Balance of fatty acids and their correlations with parameters of lipid metabolism and markers of inflammation in men with coronary atherosclerosis. *Bull. Exp. Biol. Med.* **164**, 33–35 (2017).
41. Stallings, V. A. et al. Diagnosing malabsorption with systemic lipid profiling: pharmacokinetics of pentadecanoic acid and triheptadecanoic acid following oral administration in healthy subjects and subjects with cystic fibrosis. *Int. J. Clin. Pharmacol. Ther.* **51**, 263–273 (2013).
42. Jenkins, B. et al. The dietary total-fat content affects the in vivo circulating C15:0 and C17:0 fatty acid levels independently. *Nutrients* **10**, 1646 (2018).
43. Maruyama, C. et al. Differences in serum phospholipid fatty acid compositions and estimated desaturase activities between Japanese men with and without metabolic syndrome. *J. Atheroscler. Thromb.* **15**, 306–313 (2008).
44. Yoo, W. et al. Fatty acids in non-alcoholic steatohepatitis: Focus on pentadecanoic acid. *PLoS One* **12**, e0189965 (2017).
45. Santaren, I. D. et al. Serum pentadecanoic acid (15:0), a short-term marker of dairy food intake, is inversely associated with incident type 2 diabetes and its underlying disorders. *Am. J. Clin. Nutr.* **100**, 1532–1540 (2014).
46. Galdiero, E. et al. Pentadecanoic acid against *Candida albicans*-*Klebsiella pneumoniae* biofilm: towards the development of an anti-biofilm coating to prevent polymicrobial infections. *Res. Microbiol.* **172**, 103880 (2021).
47. Ricciardelli, A. et al. Pentadecanal and pentadecanoic acid coatings reduce biofilm formation of *Staphylococcus epidermidis* on PDMS. *Pathog Dis* **78**, ftaa012 (2020).
48. Jenkins, B. J. et al. Odd chain fatty acids: New insights of the relationship between the gut microbiota, dietary intake, biosynthesis and glucose intolerance. *Sci. Rep.* **7**, 44845 (2017).
49. Dornan, K., Gunenc, A., Oomah, B. D. & Hosseini, F. Odd chain fatty acids and odd chain phenolic lipids (alkylresorcinols) are essential for diet. *J. Am. Oil Chem. Soc.* **98**, 813–824 (2021).
50. Pfeuffer, M. & Jaudszus, A. Pentadecanoic and heptadecanoic acids: Multifaceted odd-chain fatty acids. *Adv. Nutr.* **7**, 730–734 (2016).
51. Zhang, L., Liang, S., Zong, M., Yang, J. & Lou, W. Microbial synthesis of functional odd-chain fatty acids: A review. *World J. Microbiol. Biotechnol.* **36**, 35 (2020).
52. Park, Y. K., Dulerio, T., Ledesma-Amaro, R. & Nicaud, J. M. Optimization of odd chain fatty acid production by *Yarrowia lipolytica*. *Biotechnol. Biofuels* **11**, 158 (2018).
53. Rezanka, T., Kolouchova, I. & Sigler, K. Precursor directed biosynthesis of odd-numbered fatty acids by different yeasts. *Folia Microbiol. (Praha)* **60**, 457–464 (2015).
54. Zhang, L. S. et al. Using 1-propanol to significantly enhance the production of valuable odd-chain fatty acids by *Rhodococcus opacus* PD630. *World J. Microbiol. Biotechnol.* **35**, 164 (2019).
55. Wei, W. et al. *Parabacteroides distasonis* uses dietary inulin to suppress NASH via its metabolite pentadecanoic acid. *Nat. Microbiol.* **8**, 1534–1548 (2023).
56. Qin, N., Li, L., Wang, Z. & Shi, S. Microbial production of odd-chain fatty acids. *Biotechnol. Bioeng.* **120**, 917–931 (2023).
57. Wu, H. & San, K. Y. Engineering *Escherichia coli* for odd straight medium chain free fatty acid production. *Appl. Microbiol. Biotechnol.* **98**, 8145–8154 (2014).
58. Yamamoto, T., Shimoyama, T., Umegae, S. & Matsumoto, K. Tacrolimus vs. anti-tumour necrosis factor agents for moderately to severely active ulcerative colitis: A retrospective observational study. *Aliment. Pharmacol. Ther.* **43**, 705–716 (2016).
59. Torres, J. et al. Systematic Review of Effects of Withdrawal of Immunomodulators or Biologic Agents From Patients With Inflammatory Bowel Disease. *Gastroenterology* **149**, 1716–1730 (2015).
60. Bruscoli, S., Febo, M., Riccardi, C. & Migliorati, G. Glucocorticoid therapy in inflammatory bowel disease: Mechanisms and clinical practice. *Front. Immunol.* **12**, 691480 (2021).
61. Ji, Y. et al. Hydroxyproline attenuates dextran sulfate sodium-induced colitis in mice: Involvement of the NF- $\kappa$ B signaling and oxidative stress. *Mol. Nutr. Food Res.* **62**, e1800494 (2018).
62. Wu, Y. et al. Maternal galactooligosaccharides supplementation programmed immune defense, microbial colonization and intestinal development in piglets. *Food Funct.* **12**, 7260–7270 (2021).
63. Bolyen, E. et al. Reproducible, interactive, scalable and extensible microbiome data science using QIIME 2. *Nat. Biotechnol.* **37**, 852–857 (2019).
64. Noguchi, H., Park, J. & Takagi, T. MetaGene: prokaryotic gene finding from environmental genome shotgun sequences. *Nucleic Acids Res.* **34**, 5623–5630 (2006).
65. Li, D., Liu, C. M., Luo, R., Sadakane, K. & Lam, T. W. MEGAHIT: an ultra-fast single-node solution for large and complex metagenomics assembly via succinct de Bruijn graph. *Bioinformatics* **31**, 1674–1676 (2015).
66. Fu, L., Niu, B., Zhu, Z., Wu, S. & Li, W. CD-HIT: accelerated for clustering the next-generation sequencing data. *Bioinformatics* **28**, 3150–3152 (2012).
67. Li, R., Li, Y., Kristiansen, K. & Wang, J. SOAP: short oligonucleotide alignment program. *Bioinformatics* **24**, 713–714 (2008).
68. Buchfink, B., Xie, C. & Huson, D. H. Fast and sensitive protein alignment using DIAMOND. *Nat. Methods* **12**, 59–60 (2015).
69. Wick, R. R., Judd, L. M., Gorrie, C. L. & Holt, K. E. Unicycler: Resolving bacterial genome assemblies from short and long sequencing reads. *PLoS Comput. Biol.* **13**, e1005595 (2017).
70. Weiss, A. S. et al. In vitro interaction network of a synthetic gut bacterial community. *ISME J* **16**, 1095–1109 (2022).

71. Ning, L. et al. Microbiome and metabolome features in inflammatory bowel disease via multi-omics integration analyses across cohorts. *Nat. Commun.* **14**, 7135 (2023).
72. Xie, G. et al. A metabolite array technology for precision medicine. *Anal. Chem.* **93**, 5709–5717 (2021).
73. Weiss, G. A. et al. Intestinal inflammation alters mucosal carbohydrate foraging and monosaccharide incorporation into microbial glycans. *Cell. Microbiol.* **23**, e13269 (2021).
74. Chen, S., Zhou, Y., Chen, Y. & Gu, J. Fastp: an ultra-fast all-in-one FASTQ preprocessor. *Bioinformatics* **34**, i884–i890 (2018).
75. Xie, C. et al. KOBAS 2.0: a web server for annotation and identification of enriched pathways and diseases. *Nucleic Acids Res.* **39**, W316–W322 (2011).
76. Li, J. et al. *Limosilactobacillus johnsoni* and *Limosilactobacillus mucosae* and their extracellular vesicles alleviate gut inflammatory injury by mediating macrophage polarization in a lipopolysaccharide-challenged piglet model. *J. Nutr.* **153**, 2497–2511 (2023).

## Acknowledgements

This research was funded by National Natural Science Foundation of China (32125036, J.W.; 32172750, D.H.; 32330100, J.W.; and 32302765, Y.W.), Beijing Municipal Natural Science Foundation (6232024, J.W.), China National Postdoctoral Program for Innovative Talents (BX20230417, Y.W.), China Postdoctoral Science Foundation (2022M723423, Y.W.), China Agricultural Research System (CARS-35, J.W.), and 111 Project (B16044, J.W.).

## Author contributions

Y.W. performed most of the experiments and drafted the manuscript. X.Z. and X.L. analyzed the data of shotgun metagenome sequencing, 16S rRNA sequencing, RNA-seq, whole-genome sequencing and metabolomics. Q.X. and S.T. assisted with the in vitro bacterial culture experiments and animal experiments. Z.Z. provided the clinical samples. J.Z., Z.D., and D.H. commented on the study. G.Z. revised the manuscript. J.W. supervised the study and revised the manuscript.

## Competing interests

The authors declare no competing interests.

## Additional information

**Supplementary information** The online version contains supplementary material available at <https://doi.org/10.1038/s41467-024-53144-1>.

**Correspondence** and requests for materials should be addressed to Junjun Wang.

**Peer review information** *Nature Communications* thanks Lusheng Huang, Mi-Na Kweon and Andre Marette for their contribution to the peer review of this work. A peer review file is available.

**Reprints and permissions information** is available at <http://www.nature.com/reprints>

**Publisher's note** Springer Nature remains neutral with regard to jurisdictional claims in published maps and institutional affiliations.

**Open Access** This article is licensed under a Creative Commons Attribution-NonCommercial-NoDerivatives 4.0 International License, which permits any non-commercial use, sharing, distribution and reproduction in any medium or format, as long as you give appropriate credit to the original author(s) and the source, provide a link to the Creative Commons licence, and indicate if you modified the licensed material. You do not have permission under this licence to share adapted material derived from this article or parts of it. The images or other third party material in this article are included in the article's Creative Commons licence, unless indicated otherwise in a credit line to the material. If material is not included in the article's Creative Commons licence and your intended use is not permitted by statutory regulation or exceeds the permitted use, you will need to obtain permission directly from the copyright holder. To view a copy of this licence, visit <http://creativecommons.org/licenses/by-nc-nd/4.0/>.

© The Author(s) 2024